Dependency of the impacts of geoengineering on the stratospheric sulfur injection strategy part 1: Intercomparison of modal and sectional aerosol module

Anton Laakso[1], Ulrike Niemeier[2], Daniele Visioni[3], Simone Tilmes[4], and Harri Kokkola[1]

[1]Finnish Meteorological Institute, Atmospheric Research Centre of Eastern Finland, Kuopio, 70200, Finland
[2]Max Planck Institute for Meteorology, Bundesstr. 53, 20146 Hamburg, Germany
[3]Sibley School of Mechanical and Aerospace Engineering, Cornell University, Ithaca, NY, USA
[4]National Center for Atmospheric Research, Boulder, CO, USA

Correspondence: Anton Laakso (anton.laakso@fmi.fi)

Abstract. Injecting sulfur dioxide into the stratosphere with the intent to create an artificial reflective aerosol layer is one of the most studied ~~option~~ options for solar radiation management. Previous modelling studies have shown that stratospheric sulfur injections have the potential to compensate the greenhouse gas induced warming at the global scale. However, there is significant diversity in the modelled radiative forcing from stratospheric aerosols depending on the model and on which strategy is used to inject sulfur into the stratosphere. Until now it has not been clear how the evolution of the aerosols and their resulting radiative forcing depends on the aerosol microphysical scheme used, that is, if aerosols are represented by modal or sectional distribution. Here, we have studied different spatio-temporal injections strategies with different injection magnitudes by using the aerosol-climate model ECHAM-HAMMOZ with two aerosol microphysical modules: the sectional module SALSA and the modal module M7. We found significant differences in model responses depending on the used aerosol microphysical module. In a case where SO_2 was injected continuously in the equatorial stratosphere, simulations with SALSA produced 88%-154% higher all-sky net radiative forcing than simulations with M7 for injection rates from 1 to 100 $Tg(S)yr^{-1}$. These large differences are identified to be caused by two main factors. First, the competition between nucleation and condensation: while in SALSA injected sulfur tends to produce new particles at the expense of gaseous sulfuric acid condensing on pre-existing particles, in M7 most of the gaseous sulfuric acid partitions to particles via condensation at the expense of new particle formation. Thus, the effective radii of stratospheric aerosols were 10-52% larger in M7 than in SALSA, depending on injection rate and strategy. Second, the treatment of the modal size distribution in M7 limits the growth of the accumulation mode which results in a local minimum in aerosol number size distribution between the accumulation and the coarse modes. This local minimum is in the size range where the scattering of solar radiation is most efficient. We also found that different spatial-temporal injection strategies have a significant impact on the magnitude and zonal distribution of radiative forcing. Based on simulations with various injection rate using SALSA, the most efficient studied injection strategy produced 33-42% radiative forcing compared to the least efficient strategy while simulations with M7 showed even larger difference of ~~48-76~~48-116%. Differences in zonal mean radiative forcing were even larger than that. We also show that a consequent stratospheric heating and its impact on the quasi-biennial oscillation depends both on the injection strategy and the aerosol microphysical model.

Overall, these results highlight a crucial role of aerosol microphysics on the physical properties of stratospheric aerosol which
25 in turn causes significant uncertainties in estimating climate impacts of stratospheric sulfur injections.

1 Introduction

Solar radiation management (SRM) techniques are proposed to complement mitigation efforts to avoid greenhouse gas driven
catastrophic global warming (e.g. (Caldeira et al., 2013)). These techniques might be considered if major reductions in green-
house gas (GHG) emissions are not achieved or the development of efficient carbon dioxide removal techniques are delayed.
30 Instead of altering increased GHG concentration in the atmosphere, which is suppressing outgoing longwave (LW) radiation,
SRM techniques would aim to reflect more shortwave (SW) radiation from the Earth's atmosphere back to space in order to
mitigate GHG-induced changes in the net radiation flux. Even though SRM could ~~be in theory,~~ in theory, be used to mitigate
or even compensate the global mean net radiation flux changes due to GHGs, ~~it changes the structure of the Earth's energy
budget~~SW and LW radiative fluxes are zonally and vertically still different compared to those in the unperturbed atmosphere.
35 This would lead to some side effects. For example, offsetting GHG-induced warming by reflecting more radiation decreases
the global mean precipitation ((Tilmes et al., 2013; Laakso et al., 2020)) and can lead to the cooling of the tropics while high
latitudes are still warmer than before GHG-induced warming, if solar radiation is reduced uniformly (~~etc~~ e.g. percent solar
constant reduction) (Kravitz et al., 2021).

One of the most cost-efficient technique to increase the reflectivity of the Earth is continuous stratospheric aerosol interven-
40 tion (SAI) using sulfur. This technique mimics large volcanic eruptions, where a large amount of sulfur reaches the stratosphere,
subsequently forming aerosols from gaseous sulfur that form a long lasting (1-2 years) reflective blanket temporally cooling the
climate. Thus, this is the one of the few or if not the only SRM technique for which ~~we~~ have observational evidence supporting
its efficiency in cooling the climate at the global scale. However, due to the rare occurrence of large volcanic eruptions which
has long lasting climate impacts, there are good modern day observations on volcanic aerosols properties and radiative effects
45 only for one large volcanic eruption, Pinatubo in 1991. In addition, sulfur from large volcanic eruption is released to a relatively
particle free stratosphere. In the case of ~~geoengineering, stratospheric~~ SAI, sulfur injections are instead done continuously onto
existing particle field from the preceding injections. This would affect the size distribution of the stratospheric aerosols and the
following radiative and climate impacts. Thus it is not straightforward to draw conclusions about possible impacts of SAI based
on observations of large volcanic eruptions. ~~A lack of measurements have resulted in a major uncertainty on the estimations of~~
50 ~~cooling and other impacts of stratospheric sulfur injections (Plazzotta et al., 2018).~~

~~Because of the~~ Because of this nonlinear nature of aerosol evolution, together with a lack of measurements ~~, most of
the climate impact estimations of SAI rely on climate model simulations .~~ after large volcanic eruptions, the climate model
simulations are required to understand climate impacts of SAI.

There are several approaches to model SAI. In some studies, the effect of stratospheric sulfur injections are imitated by
55 decreasing the solar constant, which however is not a good proxy for radiative impacts of stratospheric aerosols (Visioni
et al., 2021). Aerosols absorb a part of the longwave radiation which has an impact on the atmospheric energy budget and

on atmospheric dynamics. In addition, the cooling potential and the spatial distribution of radiative forcing depend on aerosol microphysics and the transport of the particles. Studies where aerosol microphysics is simulated, have shown that global mean radiative forcing does not increase linearly with the amount of injected sulfur (Heckendorn et al., 2009; Pierce et al., 2010; Niemeier et al., 2011). Increasing the magnitude of the injection leads to larger particles in size with a smaller number concentration. Larger particles work as an efficient condensation sink for gaseous sulfuric acid and a coagulation sink for new particles forming via nucleation. ~~However,~~ Tilmes et al. (2018a) have shown a linear relationship between injection amount and temperature reduction of SAI. However this relation was defined based on scenarios where the background conditions were not fixed and injection strategy was changed during the simulation (see e.g. Visioni et al. (2020a)), and thus these results are not directly comparable with the above mentioned studies.

There is a large diversity in the predicted radiative forcing of ~~stratospheric geoengineering~~ SAI between studies where aerosols microphysics is simulated. For example, based on Niemeier and Timmreck (2015), the injection rate of 10 $Tg(S)yr^{-1}$ leads to -(1.79-2.06) Wm^{-2} all-sky radiative forcing at the top of the atmosphere (TOA). Based on Laakso et al. (2020), only 3 $Tg(S)yr^{-1}$ were required to induce a radiative forcing of same magnitude (-2.2 Wm^{-2}). Injecting 6 Tg(S) per year in the Laakso et al. (2020) resulted in -3.72 Wm^{-2} total radiative forcing while achieving the same cooling effect required 20 $Tg(S)yr^{-1}$ in simulations of Niemeier and Timmreck (2015). Both studies used different generation of the same general circulation model (GCM) ECHAM but the main difference was how the aerosol microphysical processes were modelled. Simulations by Niemeier and Timmreck (2015) were done with a modal aerosol model (M7) while a sectional model (SALSA) was used in Laakso et al. (2020).

In addition, Kleinschmitt et al. (2018) studied the dependency of geongineering to the magnitude of SAI using a GCM with a sectional aerosol scheme (LMDZ-S3A). Their results on net radiative forcing where close to the values in Niemeier and Timmreck (2015), but both LW and SW radiative forcing, which ~~have~~ had opposite impact on net radiation (i.e different signs), were individually significantly larger. In Niemeier and Timmreck (2015), the LW forcing efficiency (forcing per injected sulfur) were roughly 0.1 $Wm^{-2}/(Tg(S)yr^{-1})$ regardless of injection rate. SW forcing efficiency was -0.35 $Wm^{-2}/(Tg(S)yr^{-1})$ with 1 $Tg(S)^{-1}$ sulfur injection rate and decreased gradually to -0.22 $Wm^{-2}/(Tg(S)yr^{-1})$ when injection rate were increased to 50 $Tg(S)^{-1}$. In Kleinschmitt et al. (2018), the corresponding change in SW forcing efficiency was -0.5 to -0.3 $Wm^{-2}/(Tg(S)yr^{-1})$ while the LW forcing varied between 0.2 and 0.3 $Wm^{-2}/(Tg(S)yr^{-1})$. Kravitz et al. (2017) simulated injections with strengths between 1-25 $Tg(S)yr^{-1}$ with CESM1(WACCM) where the aerosol size distribution is represented using three modes. In their study, the SW forcing efficiency varied roughly from -1.0 to -0.7 $Wm^{-2}/Tg(S)yr^{-1}$ and the LW forcing from 0.7 to 0.6 $Wm^{-2}/Tg(S)yr^{-1}$. However, these fluxes were calculated from fully coupled simulations and thus are not fully comparable to the direct radiative forcing estimates of the other above-mentioned studies.

In addition to the fact that the simulated radiative effects depend on which model is used, they also depend on the injection strategy and how injections are varied spatially and temporally. There is a good agreement between studies in that when injection rates are lower than 10 $Tg(S)yr^{-1}$, increasing altitude of the injection increases the lifetime of aerosols and the radiative forcing (Heckendorn et al. (2009); Niemeier et al. (2011); Kleinschmitt et al. (2018); Vattioni et al. (2019); Tilmes et al. (2018b)), but with with higher injection rates this can be the opposite as shown by Niemeier and Schmidt (2017).

Most of the studies have simulated the impacts of injections over the Equator where yearly average solar intensity is highest. In addition, due to the Brewer-Dobson circulation it takes longer for aerosol to be transported to high latitudes, where sedimentation rate is larger than in low latitudes. Niemeier et al. (2011) showed that injecting only to one model grid box induced a stronger radiative forcing compared to when injections were performed in a band over Equator. However, based on Vattioni et al. (2019) injecting to one grid box or band over longitudes did not have a significant impact, while (Mills et al., 2017) found that injections along one longitude result in ~~larges~~ larger particles than point injections and are therefore less efficient. English et al. (2012) showed that an injection to a broader band over the Equator would increase the lifetime of sulfur, while Vattioni et al. (2019) did not find a significant impact of broadening injection area. On the other hand, Kleinschmitt et al. (2018) found that broadening the injection band had a negligible impact on the net radiative forcing but individually SW and LW forcing, which have opposite impact on the radiation, decreased by 20-30 % in the case of 10 Tg(S)yr^{-1} injection rate.

Sulfur can also be injected at ~~the~~ a certain time of the year instead of continuous injections. Heckendorn et al. (2009) and Niemeier et al. (2011) studied scenarios where injections were done twice per year. Based on Heckendorn et al. (2009), this strategy of using pulsed injections increased the forcing more than 50% compared to continuous injections. However, based on Niemeier et al. (2011) continuous and pulsed injection scenarios did not exhibit a large difference in their radiative impacts. Visioni et al. (2019) simulated single-point injections at the different latitudes only in certain season and showed that it can reduce the required sulfur for achieving a certain aerosol optical depth. The injection area can also be varied spatially depending on the season. Laakso et al. (2017) and Kleinschmitt et al. (2018) showed that this led to a slight increase of radiative forcing compared to continuous Equatorial injections, but the zonal distribution of the forcing was concentrated relatively more on midlatitudes and less over the Tropics. The sensitivity of modelled response to different spatio-temporal injection strategies can also be dependent on to the injection magnitude which has not so far been studied.

Overall, as these studies listed above show, there is a large diversity in radiative forcings of SAI between studies and differences depend on which general circulation model and microphysical module is used, how the injections are varied spatially and temporally, and what is the magnitude of the sulfur injections. Simulating aerosol microphysics is computationally heavy. This ~~has~~ sets limitations for investigating different injection scenarios with different amounts of injected sulfur. However, increased computing capacity in the last few years enables studying a wide range of different injection strategies in a feasible computation time. There are only few aerosol-climate models which include both modal and sectional approaches for representing aerosol size distribution and calculating aerosol microphysics which would allow studying how the the aerosol microphysics scheme affects the simulated impacts of ~~stratospheric sulfur geoengineering~~ SAI. Here we do comprehensive study on the radiative impacts of stratospheric sulfur injections. We use ECHAM-HAMMOZ aerosol-climate model, which includes both the modal aerosol module - M7 and the sectional aerosol module - SALSA~~.~~, . These modules have shown stratospheric aerosol loads consistent with the observations of the Mt. Pinatubo 1991 eruption (Niemeier et al. (2009); Toohey et al. (2011); Laakso et al. (2016); Kokk). Here both modules are used to study how the simulated impacts of geoengineering ~~depends~~ depend on the injection strategy and magnitude and how these results depend on the aerosol microphysical module used.

2 Models and Simulations

2.1 Aerosol-climate model ECHAM-HAMMOZ

Simulations were done with aerosol climate model ECHAM-HAMMOZ (ECHAM6.3-HAM2.3-MOZ1.0) (Zhang et al. (2012); Kokkola et al. (2018); Schultz et al. (2018); Tegen et al. (2019)). The host model is the general circulation model ECHAM6.3 (Stevens et al. (2013)). Simulations were performed with a T63L95 resolution which corresponds approximately to a $1.9° \times 1.9°$ horizontal grid. The atmosphere was divided into 95 vertical levels reaching up to ~ 80 km. This resolution enables to resolve the quasi-biennial oscillation (QBO) in the tropical stratosphere which has an impact on the transport of the stratospheric aerosols.

The aerosol module HAM is interactively coupled to ECHAM and its radiation module (Tegen et al. (2019)). HAM calculates emissions, removal, the radiative properties for the major global aerosol compounds of sulfate, organic carbon, black carbon, sea salt, and mineral dust. It includes gas and liquid phase chemistry of sulfur. ECHAM-HAMMOZ also includes the chemistry model MOZART. Using this model configuration would allow online calculation of ozone and the hydroxyl radical (OH) which is the main oxidizing agent of SO_2. However, this model configuration is computationally heavy and would triple the computational time and its impact on stratospheric sulfur field was relatively small compared to the impact of microphysical processes in our test simulations (not shown). This is because in the case of the continuous injection rates mean that only a fraction is injected each day. Thus stratospheric OH concentrations are not as depleted as in the case of large volcanic eruptions where several megatons of sulfur are dumped during few hour period. However as shown by (Richter et al., 2017) SAI has significant impact on the ozone concentration which further have impact on atmospheric dynamics and injected aerosols. Nevertheless we did not include MOZART as an active component in our simulations and OH and ozone concentrations were prescribed by a monthly mean climatology. The sea surface temperature, sea ice, as well as the atmospheric GHG concentration and aerosol emissions were fixed to year 2005 levels. The aerosol surface emissions were based on the ACCMIP (Emissions for Atmospheric Chemistry and Climate Model Intercomparison Project) anthropogenic emission inventory. Emissions for sea salt and dust are calculated online.

In this study ~~, when we discuss about "Radiative forcing" we refer~~ the term "radiative forcing" refers to the instantaneous radiative forcing', which is calculated by a double radiation call with and without aerosols and as a difference between specific SAI experiment and control simulation.

The microphysical processes of nucleation, condensation, coagulation, and hydration were simulated by the microphysical module. For this, ECHAM-HAMMOZ has two options: SALSA, where aerosols are represented by size bins of fixed width, and M7, where aerosols are represented using lognormal modes. Both modules have been shown to simulate the stratospheric aerosol loads and radiative properties consistently compared to the observations of the Mt. Pinatubo 1991 eruption (Kokkola et al. (2018)). However, when using M7 this requires ~~slight changes in model configuration~~ changes in the configuration of the mode and a narrower width of the largest mode to improve representation of the stratospheric aerosols (Kokkola et al., 2009). Thus, one downside of using a modal scheme is that tropospheric and stratospheric aerosols are not well described with the same model configuration.

2.1.1 Sectional aerosol module - SALSA

SALSA describes aerosols using 10 size bins in size space. The seven largest bins are represented separately for soluble and insoluble material. A detailed description of the SALSA is found in Kokkola et al. (2018). ~~For this study, we made one change to the definition of size bins in the the default setup in SALSA (Kokkola et al., 2018).~~ SALSA bins are divided into subregions, where the first subregion covers the three smallest bins and the second subregion covers the rest of the seven larger bins. The particle size distribution (i.e moving particles from one size bin to another) is updated (at each time-step) based on the mean volume of the bin assuming that aerosols in the bin are evenly distributed and on the actual mean volume of the particle population (calculated based on the mass and number of aerosols) in the corresponding bin, after the microphysical processes have been calculated. If the actual mean volume of the particle population is larger than the mean volume of the monodisperse size bin, a certain part of the aerosol population is moved to the next bin. This method is called hybrid bin (Young (01 Oct. 1974),Chen and Lamb (15 Sep. 1994)). The scheme for new particle formation ~~scheme uses~~ is based on the Kerminen and Kulmala (2002) J3 parametrization, which produces aerosols with a diameter of 3 nm. 3 nm diameter is also the lowest bound for the SALSA size distribution in the standard setup. Thus, the produced 3 nm particles are smaller than the volume mean diameter of the smallest bin in the default configuration. In the case where new particle formation is efficient, the produced 3 nm particles might keep the actual mean diameter of the smallest bin low. This prevents particles in the bin to be moved to the next bin. This led to an very high number concentration in the smallest bin in our first preliminary simulations. This was solved by changing the lower bound ~~the~~ size range of the first subregion (three smallest bins) from 3 nm to 1.02873 nm so that the volume mean diameter of smallest bin was the same as the diameter of the newly formed particles (3 nm). This lead to a smaller number concentration in the smallest size bin and a clearly higher concentration in second smallest bin. A change in the lower bound of the first subregion was the only change which was made to the default setup in SALSA (Kokkola et al., 2018).

2.1.2 Modal aerosol module - M7

In M7, aerosols are represented using a superposition of seven log-normal modes, 4 for soluble (nucleation, Aitken, accumulation and coarse) and 3 (Aitken, accumulation and coarse) for insoluble material. A detailed description of M7 is found in Vignati et al. (2004) and M7-configuration of ECHAM-HAMMOZ in Tegen et al. (2019). The original modal setup is designed to represent tropospheric conditions which is not representative for cases where the lifetime of particles is long (>months) e.g in case of the ~~stratospheric sulfate aerosol intervention~~ SAI (Kokkola et al., 2009). Similarly to Niemeier and Timmreck (2015), we modify the setup of the modes so that the coarse mode is made narrower than in the standard setup (using standard deviation σ_{CS} = 1.2 instead of 2.0)~~and the threshold radius when aerosols from the accumulation mode are transferred to the coarse mode is changed from 0.5 μm to 0.2 μm~~. In case of high sulfur concentrations, a 2.0 μm coarse mode width has shown to lead to a tail of large particles (Kokkola et al., 2009). Based on Kokkola et al. (2009) this caused an overestimation of the effective radius of the coarse mode, when compared to the highly resolved particle spectrum reference model, and thus increased sedimentation velocity and reduced residence time of aerosols. In M7 the median size of the mode can change, but only between mode specific maximum and minimum threshold radii. For the nucleation mode there is no lower threshold

radius and for coarse mode there is no higher threshold radius. This threshold radius also defines when aerosols are transferred from one mode to another. As in Niemeier and Timmreck (2015) we changed this threshold radius between accumulation and coarse mode (the two largest modes) 0.5 μm to 0.2 μm. Our model setup does not include ~~all modifications done in (Niemeier and Timmreck, 2015) e.g. the simple stratospheric sulfur scheme~~additional stratospheric chemistry, limitation of available OH for oxidation of SO_2 in extreme high SO_2 concentration (> 1000 Tg (S)) and forced evaporation of sulfate over 30 km as in Niemeier and Timmreck (2015) and Niemeier et al. (2021). Even though the mode setup of the model was modified to represent well the stratospheric aerosol at the expense of representation of the tropospheric aerosols (especially sea salt and dust), we also include all anthropogenic emissions and natural surface emission.

2.2 Scenarios

Studied scenarios are listed in Table 1 and were simulated with both SALSA and M7 aerosol modules. In addition, the control (*CTRL*) simulation without SAI was simulated with both microphysics models. In our *Baseline* scenario, sulfur was injected at 20-22 km altitude (3-4 model vertical levels) and a band across all longitudes between the latitudes 10° N and 10° S. To study the sensitivity of radiative forcing to the magnitude of the injection, the yearly injection rates of 1, 2, 5, 10, 20, 50, 100 Tg(S) were used. In addition, we simulated eight sensitivity scenarios with alternative injection strategies (see supplement fig S1). These were done for injection rates 2, 5, 20 and 50 Tg(S)yr^{-1}. Scenarios *Narrow* and *Wide* were simulated to study the impacts of shrinking or widening the injection area. In the *Narrow* scenario, injections are done between the latitudes 1.9° N and 1.9° S (two grid boxes wide band) and to 21 km altitude (one model vertical level) and in *Wide* scenario sulfur is injected between the latitudes 30° N and 30° S and same altitude as in *Baseline* scenario. Scenarios *Low* (injections at 18-20 km altitude) and *High* (injections at 22-24 km altitude) were done to study the dependency of radiative forcing on altitude. We also simulated two scenarios ~~,~~where injections are concentrated on ~~the~~certain times of the year ~~and not continuously~~instead of having continuous emissions over a year. In ~~this case the concentration of injected sulfur is larger compared to the continuous injections with same yearly injection rate, but on the other hand, there are times when injections are suspended and sulfate aerosol field is not under new injections. This might affect on the size distribution of the stratospheric aerosols. In~~both of these scenarios the length of the one injection period is one month. In *~~Pulse2m~~Pulse-eom*, sulfur was injected ~~in during every two months~~every other month starting from January ~~. In~~(6 injection periods per year). In *~~Pulse6m~~Pulse-Jan-Jul* scenario, sulfur was injected during two single months per year, January and July. In these cases, the concentration of sulfur during injections is higher compared to the *Baseline* scenario which has a constant injection rate throughout the year. Instead, in scenarios *Pulse-eom*, and *Pulse-Jan-Jul*, injections are interrupted outside the injection periods. This might affect the size distribution of the stratospheric aerosols.

In *Seasonal* scenario, 20° wide injection area is varied gradually between 40° N and 40° S throughout the year ~~similarly to Laakso et al. (2017)~~. The northernmost position (40° N - 20° N) of injection area is in May and the southernmost position (20° S - 40° S) is in November (see Fig S1). Note that ~~results~~as injection band is always 20 ° latitudes wide and a same mass in injected in every month, concentration of injected sulfur is smaller at the times when injection area is located over the Equator compared to times, when it is over midlatitudes. Results of scenarios *Seasonal* or *~~Pulse6m~~Pulse-Jan-Jul* are also

Table 1. Simulated scenarios - Linestyles and markers used to indicate scenarios in the figures are shown beside the corresponding scenario name. SALSA *Baseline* results are colored in blueish and M7 results by reddish colors in sect. 3.1 and in black in sect. 3.3. Injections are done across all longitudes between stated latitudes in all other scenarios other than the Point scenario.

Baseline		
SRM1-100	————	continuous 1, 2, 5, 10, 20, 50 and 100 Tg(S)/yr SO$_2$ injections to 10° N - 10° S and 20-22 km
Sensitivity		**2, 5, 20 and 50 Tg(S)/yr SO$_2$ injections**
Narrow	·–·–●·–·	1.9° N - 1.9° S and 21 km, continuous
Wide	·–·–●·–·	30° N - 30° S and 20-22 km, continuous
High	–▲–	10° N - 10° S and 22-24 km, continuous
Low	–▼–	10° N - 10° S and 18-20 km, continuous
~~*Pulse2m*~~*Pulse-eom*	····■····	10° N - 10° S and 20-22 km, injection ~~every two months~~ in every other month
~~*Pulse6m*~~*Pulse-Jan-Jul*	····⬟····	10° N - 10° S and 20-22 km, injection ~~every six months~~ only in January and July
~~*Onegb*~~*Point*	–·●·–	Injections to ~~two gridbox~~ one gridbox (1.9° N - 0) at the Equator, 21 km, continuous
Seasonal	—S—	20° wide area varies seasonally between 40° N and 40° S, north most position at May, 20-22 km, continuous

sensitive to the timing of injections which, however, are not studied here. ~~One sensitivity scenario was~~ The last of the studied sensitivity scenarios was ~~*Onegb*~~*Point*. There, sulfur was injected only in one ~~meridional grid box~~ grid box located in prime meridian instead of a band over all longitudes~~, and to have a symmetry between hemispheres, and regardless of the name of the scenario, to two grid boxes closest to the Equator. These two grid boxes were located in prime meridian~~.

Simulations were run over a 10 year period which included a 3-year spin-up period. Thus a 7 year period was used in the analysis. The period length of 7 years was chosen because it covers roughly three full QBO cycles (3 x 28 months = 7 years).

3 Results

3.1 *Baseline* scenarios - Sensitivity to magnitude of injections

3.1.1 The dependency of radiative forcing on the amount of the injected sulfur

Figure 1 shows the dependency of the global mean All-sky SW and LW radiative forcing, the stratospheric sulfur burden, and the effective radii of aerosols on the magnitude of sulfur injection in the scenario *Baseline*. The results of SALSA are shown by reddish lines and markers, M7 results are indicated by blueish color. The SW radiative forcing increased and the forcing efficiency decreased sub-linearly with the injection rate in both models. However, the increase in LW forcing was rather linear as a function of the magnitude of injected sulfur (Fig. 1b). This was consistent between models. Overall, because SW forcing was significantly larger than LW forcing, the net total forcing was always more negative (stronger cooling effect). However,

in the case of stronger injections (> 5 Tg(S)yr^{-1}) LW forcing contribution to the total forcing becomes relatively higher especially in simulations with M7. Thus, for example the change in the total forcing in simulations with M7 was rather small (-2.09 Wm^{-2}) even though the amount of injected sulfur was doubled from 50 to 100 Tg(S) (Fig. 1c). Several studies have shown that a stronger sulfur injection will lead to relatively larger aerosols (Heckendorn et al. (2009), Pierce et al. (2010), Niemeier

245 et al. (2011), Laakso et al. (2016)). This happens also here regardless of how the aerosol microphysics is modelled. This is supported by Fig. 1d which shows that the area-weighted mean stratospheric effective radius was increased with increasing injections.

Even though the same qualitative conclusions about the behaviour of the efficiency of SAI as a function of the amount of injected sulfur can be drawn based on both SALSA and M7 microphysical modules, the quantitative results between the models

250 were significantly different. The SW radiative forcing was 45-85% higher in SALSA than in M7. ~~In~~ On the other hand the LW radiative forcing was 32-67% higher in M7 than in SALSA. As impact on net radiation is opposite between the SW and LW radiative forcing of aerosols, this led to an even larger difference in the total net radiative forcing between models as can be seen in Fig. 1c. With 1 Tg(S)yr^{-1} and 2 Tg(S)yr^{-1} injection rates, the total radiative forcing was 88% and 117% higher in SALSA than in M7. In the case of higher magnitude injections (5-100 Tg(S)yr^{-1}), the net radiative forcing was 137-154%

255 based on simulations with SALSA than with M7. Thus, the efficiency of stratospheric sulfur geoengineering was significantly dependent on the aerosol module used.

The net radiative forcing in our M7 simulations was in very good agreement with the results of Niemeier and Timmreck (2015) which are indicated with black dashed line in Fig. 1c. This was at least partly a coincidence, even though M7 with a similar mode setup was used here as in Niemeier and Timmreck (2015). Niemeier and Timmreck (2015) used ECHAM5-

260 HAM instead of ECHAM6.3-HAM2.3 which was the case in our study. Niemeier and Timmreck (2015) simulations were done using 39 model vertical levels instead of 95 and the injection altitude was 19 km which was thus a lower altitude than in our simulations. In addition, the sulfur was injected to the one grid box instead of injecting along the Equator which was the case in our simulations. If the SALSA results presented here are compared with the results of Kleinschmitt et al. (2018), where a sectional aerosol module with 36 size bins between dry radii 1nm and 3.3nm was used, we see a significant difference

265 especially in the LW radiation response. In the case of stronger than 5 Tg(S)$^{-1}$ injection rates, our simulation showed the LW forcing efficiency to be lower than 0.1 Wm^{-2}/Tg(S)yr^{-1} while in Kleinschmitt et al. (2018) it was approximately 0.3 Wm^{-2}/Tg(S)yr^{-1}. This means that the LW forcing was more than two times larger in Kleinschmitt et al. (2018) than in our simulations. Ozone were prescribed in Kleinschmitt et al. (2018) as also in this study and thus different responses in LW forcing cannot be explained by different response of ozone on SAI. The SW forcing efficiency was slightly larger in SALSA

270 simulations with the 1-2 Tg(S)yr^{-1} but with stronger injection rates, the results are consistent with those of Kleinschmitt et al. (2018). The dry effective radii of stratospheric aerosols with different injection magnitudes were nearly identical between the studies. This indicates that differences in radiative forcings between the studies are probably caused by differences in the LW radiation transfer, i.e in using a different radiative transfer scheme, or differences in the aerosol optical properties in LW radiation calculations. In addition, in Kleinschmitt et al. (2018) radiative properties of aerosols were calculated from

275 a prescribed chemical composition consisting of 75% H$_2$SO$_4$, while in SALSA volume-weighted average of the refractive
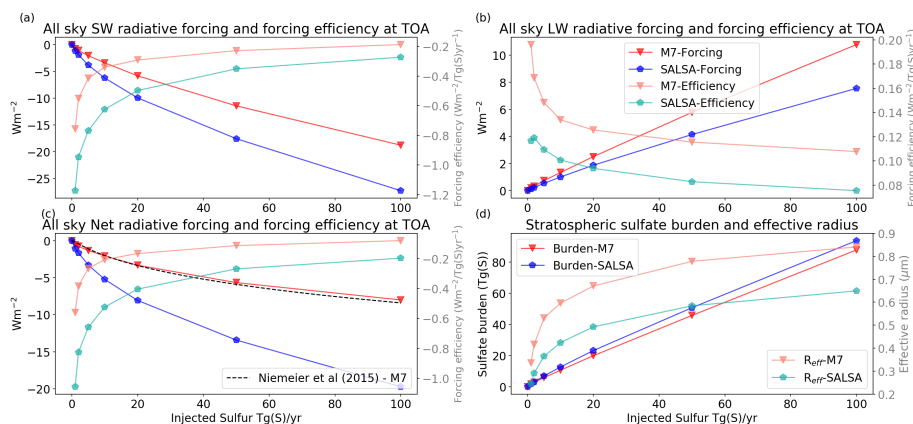
Figure 1. Global mean all-sky a) shortwave, b) longwave and c) total (net) radiative forcing and forcing efficiency and d) stratospheric sulfate burden and the mean effective radius as a function of injection rate. M7 results are shown by red lines and markers and SALSA results are indicated by blue color.Faint colors (forcing efficiency in a)-c) and effective radius in d)) correspond to the right-hand faint axis.

indices of individual compounds is used. However, it can also be that the size-distribution of aerosols were different regardless of having consistent effective radii, or how aerosols are spatially distributed in atmosphere.

Despite the fact that the radiative forcing was significantly different here between M7 and SALSA, the stratospheric sulfur burdens were only 3-19% higher in SALSA than M7. ~~This indicates that there were fewer~~ Lower SW radiative forcing, higher
280   LW radiative forcing and a slightly shorter lifetime is caused by less and larger sulfate particles in M7 simulations than in SALSA. This conclusion is justified by examining the stratospheric mean effective radii (the light blue and red lines) in Fig. 1d. To analyze the aerosol size in more detail, the number size distribution along the Equator at 20-22 km of altitude in M7 and SALSA simulations for ~~5 and 50 Tg(S)yr^{-1}~~ different injection rates are shown in Fig. 2. The total number concentrations were larger in SALSA than in M7 in all size classes except in particles with diameter larger than 0.7 μm. Note that in the case of
285   the ~~50 Tg injections~~largest injection rates, a part of the aerosols is present in the largest bin (of size range 1.7-4.12 um), whose upper size limit goes beyond the coarse mode in M7. However, the actual mean aerosol size for that bin (~~blue~~ purple circle in the bin) is closer to its lower limit, unlike in the other bins.

To understand the link between the size distribution and the radiative forcing we reproduced an indicator for size range where the backscattering efficiency is highest, similarly to Figure 5 of Vattioni et al. (2019). Defined size range is based on Dykema
290   et al. (2016). The size range is shown as a ~~light green~~grey shaded area in Fig. 2. The magenta line shows the dependency of the LW absorption for radiation with wavelength of 8000 nm to the size of sulfate aerosol calculated using the SALSA radiation module for aerosols (absorption is shown here as an unitless quantity, the scale is linear). In SALSA, the aerosol number concentration was much higher than in M7 over the the size range of highest backscattering. On the other hand, high number concentration at the largest size range (>0.7 μm) in M7 caused stronger LW radiative forcing than the LW forcing calculated
295   for the SALSA simulated size distribution. Figure 2 shows clearly why the net radiative forcing increases (becomes more
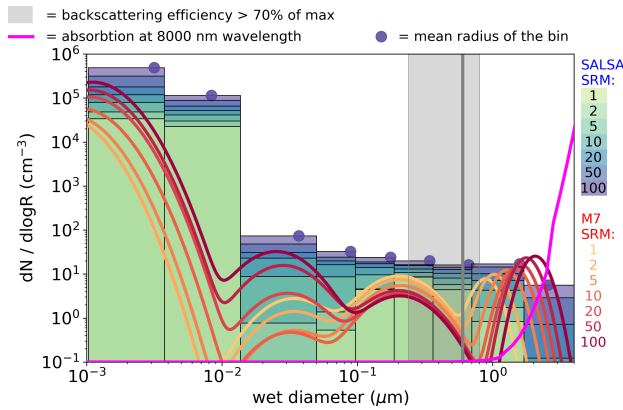
Figure 2. Aerosol number size distribution at the Equator and at the 20-22 km altitude in scenarios ~~SRM5 and SRM50~~ with different injection rates simulated with M7 (names of the four modes from the left: Nucleation, Aitken, Accumulation, Coarse) and SALSA (10 size bins, there is no significant number of aerosols in largest bin, and thus it is not shown in the figure.). Dots on the top of the SALSA size bins show the mean diameter of that bin in the case of 100 Tg(S)yr^{-1} injection rate. The ~~light green~~ grey line is reproduced from Figure 5 of Vattioni et al. (2019) and shows the size for which the back scattering is maximized. ~~Shaded~~ Grey shaded area indicates radius where aerosol backscattering is 70 % of the maximum Dykema et al. (2016). Magenta line shows (~~here shown as a~~ unitless~~quantity~~) ~~shows~~ the relative dependence (in a linear, not logarithmic scale) of absorption of 8000 nm wavelength on the (dry) diameter of the sulfate aerosols, and is based on the radiation calculation module of SALSA.

negative) faster in SALSA than M7. When the injection rate was increased~~from 5 to 50 Tg(S)yr^{-1}~~, the number concentration was increased in all size bins in SALSA. However, in M7 ~~changes in~~ number concentration of the accumulation mode ~~were small~~aerosols were decreased. On the other hand, the number concentration of the coarse mode was increased and it grew in size. As seen in Fig. 2, this change is critical for LW radiative forcing because the absorption efficiency increases strongly with the aerosol size when the aerosol diameter is larger than 1 μm.

Compared to the aerosol size distribution in Niemeier and Timmreck (2015), ~~it~~ the size distribution based on M7 simulations in our study was considerably different~~in our M7 simulations~~. The number concentrations of Aitken and Accumulation modes were much larger in Niemeier and Timmreck (2015) and the amount of accumulation aerosols was increasing with larger injections. These differences are probably explained by the different injection strategy. As we will show in sect. 3.3.2 the scenario where sulfur is injected to one model grid box as in Niemeier and Timmreck (2015) results in the more consistent aerosol size distribution (Fig. ~~S5b~~ S7b in supplement) with Niemeier and Timmreck (2015). In addition, the difference between our study and Niemeier and Timmreck (2015) is a different version of the ~~same GCM and a different resolution was used here, resulting in~~ GCM and different ~~atmospheric dynamics~~ resolution used in the model. Niemeier and Schmidt (2017) have shown that low and high vertical resolutions led to different stratospheric dynamics which further caused differences in aerosol sizes in SAI simulations.

3.1.2 Dependency of zonal distribution of radiative forcing on the amount of the injected sulfur

Figure 3 shows the zonal distribution of the relative clear sky SW and LW radiative forcings (i.e. zonal~~forcing~~/global mean radiative forcing). The maximum of the zonal mean radiative forcing was concentrated on latitude bands within the injection region (the shaded area in Fig. 3) over the Equator in both models and regardless of the magnitude of injections. There were also two local maxima: both 50° N and 50° S latitudes especially in the zonal SW radiative forcing. When the injection rate was increased, the relative radiative forcing at high latitudes decreased and the above-mentioned local maximas of the SW radiative forcing at 50° latitudes had moved towards low latitudes. Consequently, the relative radiative forcing increased in the tropics and subtropics while it decreased over higher latitudes. This was consistent between the models. There are two explanation for this: 1) when the amount of sulfur was increased, aerosols became relatively larger, thus having higher gravitation settling velocity which means that fewer particles made it to high latitudes and 2) as it has been shown, injected sulfate aerosols ~~can strengthening~~ cause tropical stratospheric heating and a strengthening of the polar vortex~~with higher tropical stratospheric heating, preventing particles from reaching~~, which reduces aerosol transportation to the polar stratosphere (Visioni et al. (2020a) see also sect. 3.4). Thus, less sulfate aerosols were transferred to high latitudes before they were removed from the atmosphere. The variation seen in the LW radiative forcing with low injection rates (1-2 Tg(S)yr^{-1}) is caused by background aerosols and the variation in the emitted LW radiation from the atmosphere and the surface due to land temperature adjustments.

The zonal mean effective radii were notably different between the models (Fig. 4). The impact of the injection area on the aerosol effective radii is clearly seen in SALSA between latitudes 10° N to 10° S, where the zonal mean effective radius over the injection band was smaller than over the higher latitudes. This indicates that continuous injections were resulting in continuous new particle formation in SALSA. When particles were transferred out from the injection area, the effective radius began to rise due to particle growth by coagulation and condensation, while less new particles were produced by nucleation. In M7 simulations, the effective radii were much larger over the tropics than over high latitudes. This indicates that more of the injected sulfur has condensed on pre-existing particles rather than forming new particles inside of injection area.

Figure 5 shows the aerosol number size distribution over the latitudes 20 °N and 50 °N. When the aerosol plume moved towards high latitudes, the number of the Aitken and accumulation mode aerosols began to increase and coarse mode to decrease compared to the size distribution over the Equator. Thus, the aerosol effective radii over latitudes 20 °N and 50 °N were much smaller compared to effective radius at the Equator. In SALSA, the number size distribution at 20 °N and 50 °N is three modal in shape while at the Equator, excluding two smallest bins, it was relatively monodisperse. At the 50 °N latitude the number size distribution and effective radius were more consistent between models than closer to the injection area. However, there is still a gap between accumulation and coarse modes in M7.

In addition to radiative impacts, the size of the aerosols affects where and how fast particles are removed from the atmosphere. As Fig. ~~S1~~ S2 in the supplement shows, deposition at the tropics was much faster (32% in 50 Tg(S)yr^{-1} injection rate) in M7 than in SALSA while the deposition of sulfur outside the tropics was ~~slower~~ lower (roughly 10% in SRM50). This conclusions holds regardless of the amount of injected sulfur. ~~Simulations were too short to make a statistically significant detailed analysis of geographical distribution of deposition in the case of lower than 10 Tg(S)yr^{-1} injections due to the deposition of~~
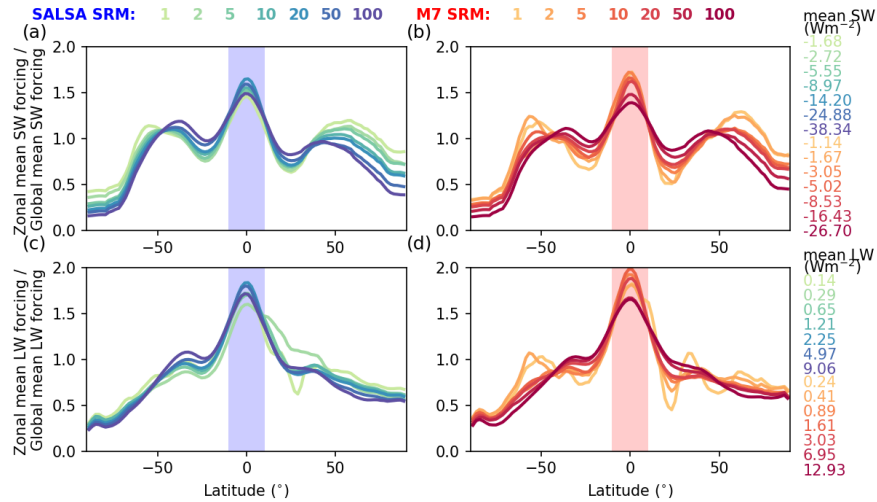
Figure 3. Relative zonal distribution of a-b) shortwave and c-d) longwave clear sky radiative forcing. Zonal mean forcing in each latitude band is divided by global mean radiative forcing of corresponding scenario which are shown in the legend right side of the figure. Blue and red shaded areas show latitudes where sulfur is injected
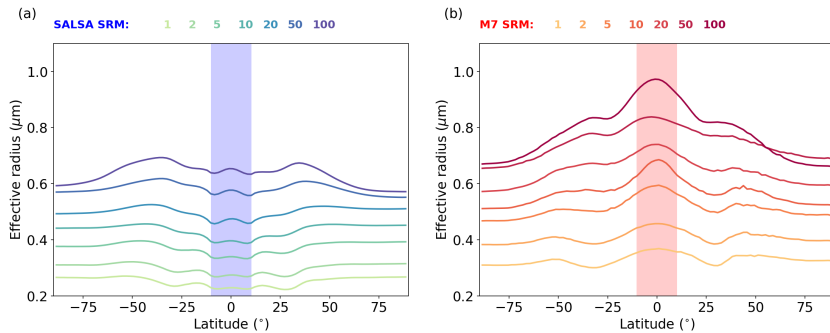
Figure 4. Dependence of the zonal mean effective radius of stratospheric aerosols on the magnitude of sulfur injections simulated with a) SALSA and b) M7. Blue and red shaded areas show latitudes where sulfur is injected

345 ~~the background sulfate aerosol. However, an estimation could be done based on the highest injection rates even though they present probably unrealistic extreme scenarios. Figure S2~~ Figure S3 in supplementary material shows that, in the case of 50 Tg(S)yr^{-1} injection rate, the deposition of sulfate is clearly faster in SALSA than M7 e.g. over Europe and United States. An enhanced sulfate deposition due to the SAI might offset or even exceed impacts of reduction of anthropogenic SO_2 emissions which might have negative impact on ecosystems in these regions Visioni et al. (2020b).
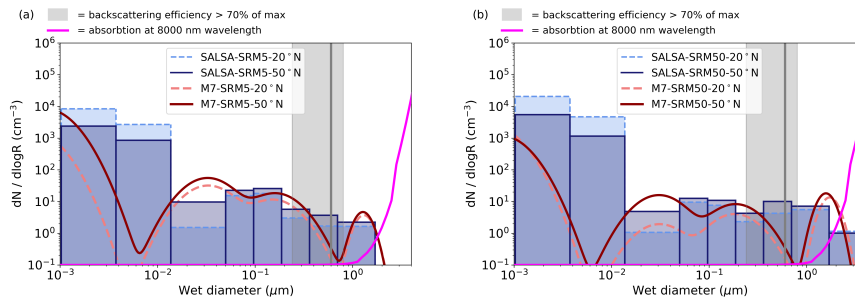
Figure 5. Aerosol number size distribution at the ~~a)~~ 20° N and 18-20 km altitude and ~~b)~~ 50° N latitudes and 12-15 km altitude in scenarios a) SRM5 and b) SRM50 simulated with M7 and SALSA. ~~Dots on the top of the SALSA size bins are showing a mean diameter of the bin. Light green~~ Grey line is reproduced from from figure of Vattioni et al (2019) and shows to size of the maximum back scattering and shaded area indicates radius where aerosol backscattering is 70 % of maximum Dykema et al. (2016). Magenta line shows (unitless) relative dependence (in a linear, not logarithmic scale) of absorption of 8000nm wavelength on the (dry) diameter of the sulfate aerosols, based on the radiation module of SALSA.

3.2 Analysing the causes for differences in results between SALSA and M7

Based on Fig. 4, there was a significant difference in the evolution of aerosols within the injection band between the two models. In there, large amounts of gaseous H_2SO_4 is constantly produced from continuous SO_2 injection and oxidation with OH. In the stratosphere the conditions are favorable for new particle formation through H_2O–H_2SO_4 binary nucleation but on the other hand, there is also a large amount of pre-existing sulfate aerosols to which gaseous H_2SO_4 can condensate. These two processes compete for available gaseous H_2SO_4 and solving them simultaneously in the model is challenging especially when sulfur concentration is high, and can lead to large biases (Kokkola et al., 2009; Wan et al., 2013). SALSA and M7 allocate the amount of sulfuric acid partitioning from gas to particles between new particle formation and condensation differently. Based on the results, in SALSA most of the gaseous sulfate is partitioned into new particle formation, while few goes into condensation. In addition, in SALSA there is a condensation sink due to a high number of particles smaller than 10 nm which ~~also prevents~~ does not exist in M7 and thus there is less gaseous sulfuric acid ~~from condensing~~ to condense to the larger particles. On the other hand, the number concentration of particles smaller than 10 nm at the Equator in M7 was only 34% of the number concentration in SALSA and, as Fig. 4 shows, in M7 the effective radius was larger inside the injection region compared to latitudes where injections did not take place. This indicates that new particle formation is much lower in M7 than SALSA and that sulfate gas condensates onto existing particles inside the injection area, which results in a larger number and size of coarse mode particles compared to latitudes where no injection is taking place.

In M7, the coupling of nucleation and condensation is done by a two-step time integration scheme proposed by Kokkola et al. (2009). Based on Wan et al. (2013) this has shown to cause negative bias for the nucleation sink and positive bias for the condensation rate. In SALSA, the operator splitting technique ~~((Jacobson, 2002))~~ (Jacobson, 2002) is used (Bergman et al., 2012). In this method, nucleation rate is added to the condensation mass transfer rate in the first size bin. Based on

370 the test simulations with the box model (not shown), when nucleation takes place, it ~~overruns~~ out-competes condensation and there is significantly less condensation. This conclusion is supported by Fig. 4a, which shows that there the effective radius is clearly smaller inside latitudes where injections take place, compared to higher latitudes. It is not clear if this is caused by overestimation of the nucleation rate, underestimation of the condensation rate, or the method used for solving nucleation and condensation simultaneously. However, to study how large an impact from the competition between nucleation

375 and condensation have on different results between models we did additional simulations where the competition is excluded in both models. These results are shown in Appendix. In these simulations, nucleation was switched off and 25% of injected sulfur mass was assumed to be primary particles 3 nm in diameter while the rest of the sulfur was injected as SO_2. ~~These~~ With the original setup, 5 Tg(S)yr^{-1} or higher injection rates simulated with SALSA showed 137-147% larger global mean all sky net radiative forcing than M7. When nucleation was replaced by injecting 25% of injected sulfur as 3nm particles,

380 radiative forcing was now only 78-99% larger in SALSA than M7. Thus, these simulations showed that excluding nucleation brought the global mean net radiative forcing results between the models closer to each other~~. However,~~, although a significant difference remained. This is because there is not a large difference in aerosol number size distribution for particles larger than 0.1 μm aerosols between *Baseline* simulations and modified simulations without nucleation (see appendix Fig. A3). Thus the most of the differences in raditive forcings between models are not caused by differences in calculating competition between

385 nucleation and condensation.

In M7, aerosol ~~sizes~~ sizeclasses are more restricted to the definition of the modes than in SALSA with bins. In M7, the mode widths are fixed~~and the~~. The mean radius of the each mode ~~have~~ can change but it has fixed low and high limits. E.g in setup used in this study, accumulation mode (second largest mode) has low and high radius limits of 0.05 and 0.2 μm respectively. These limits define average mass of the mode. If the average mass of the particles in the mode is exceeding ~~the defined average~~

390 ~~mass based on~~ average mass defined from lower and upper limits, the transfer of number and mass is done to the next mode. The impact of this can be seen ~~e.g~~ in Fig. 2. In ~~simulations with both 5 and 50 Tg(S)$^{-1}$ injection rates~~all M7 simulations regardless of injection rate, the average mass of the accumulation mode ~~(third mode from the left)~~ was close to the upper limit~~of mode and thus~~. Thus it cannot grow by condensation or coagulation because gained extra mass is always transferred to coarse mode~~which also decrease~~. This also decreases the number of accumulation mode particles. The number concentration

395 of accumulation mode can only increase by coagulation of two smaller particles or through the growth of the Aitken mode. However because coagulation between larger and smaller aerosols are more efficient than between two small aerosols, and because the number of coarse mode particles is ~~relatively~~ high, the Aitken mode cannot compete with the ~~Coarse~~ coarse mode as an coagulation sink for nucleation and Aitken mode aerosols. ~~This lowers growing of the~~ Thus less Aitken mode aerosols can grow to the accumulation mode size by coagulation. This creates self-reinforcing loop when number and mass of coarse

400 mode increases.

Because size range of accumulation mode is restricted by upper limit while coarse mode aerosols is getting larger with the larger injection, there is a gap in size distribution between these two modes where the aerosol number concentration is low (Fig. 2). Coincidentally this gap is located at the size range of the largest backscattering efficiency, which is indicated by ~~green~~ grey shaded area in Fig. 2. Thus the modal setup of M7 causes a numerical limitation for particle size distribution which, in

405 this case, have an impact on efficiency of SAI. Note that based on the earlier SAI simulations by M7 Niemeier and Timmreck (2015), the threshold radius when aerosols from accumulation mode is transferred to coarse was set to 0.2 μm (0.5 μm in standard setup).

The above-mentioned differences in the responses between models can easily go unnoticed when models are evaluated against measurements after a large volcanic eruption. Because Pinatubo is the only large volcanic eruption, which has taken
410 place during time, when proper observations about radiative properties of stratospheric aerosols are available, it has often used as a test case for models capability to simulate stratospheric aerosols (eg. (English et al., 2013; Mills et al., 2017; Niemeier et al., 2009; Laakso et al., 2016; Sukhodolov et al., 2018)). However, based on our results, it probably does not give a reliable picture of the model capability to simulate stratospheric sulfur injections for ~~SRM~~SAI. For example both models used here have shown to represent effective radius of sulfate aerosols and the burden of sulfur after Pinatubo eruption relatively well
415 (Niemeier et al., 2009; Laakso et al., 2016), and especially results were shown to be very good agreement with each other (see Figure 16 in Kokkola et al. (2018)). Still the model responses in case of SAI are significantly different. This is because background conditions in case of volcanic eruption and continuous sulfur injections are significantly different. While in case of the volcanic eruption, sulfur is erupted in a relatively particle free stratosphere, in case of SAI, sulfur is injected into existing particle field in the stratosphere. In the former case competition between nucleation and condensation does not have as large
420 role as in case of SAI. The gap in the size distribution is also widened as a consequence of continuous injections band across all longitudes when the accumulation mode cannot grow while the coarse mode is getting larger due to continuous injections. The gap is narrower in case of point-like injections as we see in the next section. This also indicates that such a clear gap as in our *Baseline* scenario does not occur in a simulation of the large volcanic eruption.

3.3 Sensitivity scenarios - Sensitivity to injection strategy

425 In this section we investigate the impact of various injection strategies on the geoengineering efficiency and the zonal distribution of the radiative forcing and how the responses depend on the model used. The descriptions of the sensitivity scenarios are found in Table 1. Fig. 6 shows the relative difference in the global mean clear sky SW, LW, and net radiative forcing compared to the *Baseline* scenario for a corresponding injection magnitude. The relative sulfate burdens compared to the *Baseline* scenario and the effective radii of stratospheric aerosols are shown in Fig. 7, while the tabulated values are given in the supplement
430 (Tab S1-2). The zonal mean net clear-sky radiative forcing is shown in Fig. 8. The zonal mean effective radius of stratospheric aerosols is shown in Fig. 9. We show here the clear-sky radiative forcing instead of all-sky, because in clear sky conditions it is more straightforward to compare the radiative forcings to the aerosols size as clouds do not affect the results. Figures for all-sky radiative forcings and tabulated absolute values of clear sky and all sky SW, LW and net radiative forcings are shown in the supplement (Fig ~~S3~~S4-5 Tab S1-2).

3.3.1 Sensitivity to the width of the injection area

To investigate the sensitivity of radiative impacts of ~~geoengineering~~ SAI to the width of the injection area, we studied injection of sulfur to bands with widths of 4° (*Narrow*), 20 ° (*Baseline*) and 60 ° (*Wide*) over the Equator. Responses of the radiative
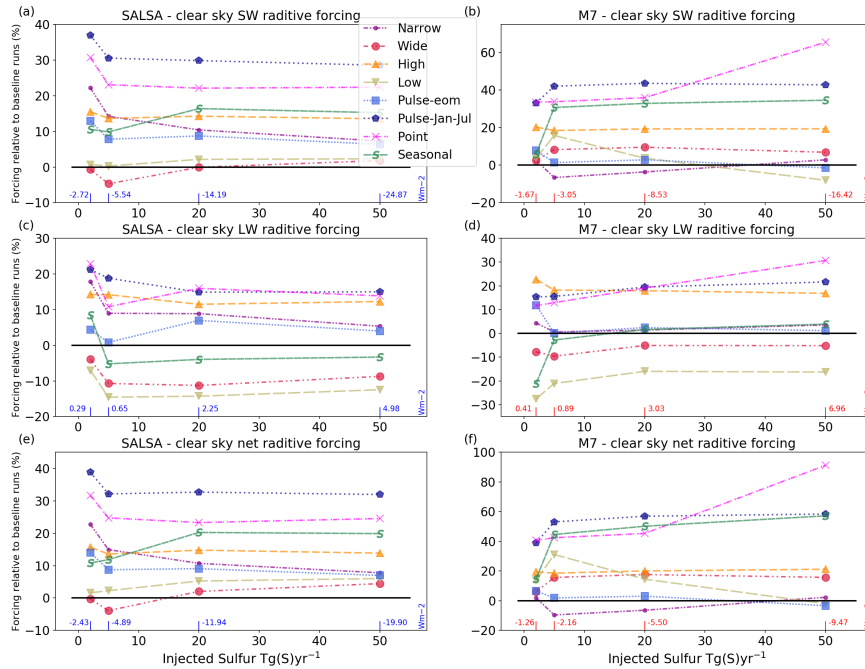
Figure 6. Relative global mean clear sky SW (a-b), LW (c-d) and net radiative forcing in sensitivity scenarios compared to *Baseline* scenario with corresponding sulfur injection rate. *Baseline* values are shown at the bottom of each panel. SALSA results are shown in the left and M7 in the right panels. Note the different y-axes scale between the panels.

forcing to the widening of the injection area from 20 to 60 ° were similar in both models. The effective radii of stratospheric aerosols were smaller and the LW radiative forcing was lower in both models compared to the *Baseline* scenario. Widening

440   the injection area affects the radiative forcing in two ways. It decreases the mean sulfate concentration over the tropics and it results in relatively more and smaller particles. These effects are shown as smaller effective radii (Fig. 7) and lower absorption of LW radiation by the smaller particles. On the other hand, injecting sulfur farther from the Equator, where the solar intensity is largest on average, decreases the potential of aerosols to scatter radiation. Widening the injection area decreases also the lifetime of aerosols because some of the aerosols are injected closer to high latitudes where they are removed faster than over

445   the low latitudes. In SALSA, where the condensation on the existing particles is weaker than in M7, concentrating sulfur injection to wider area does not matter as much as in M7 in microphysical sense, because nucleation happens at the expense of condensation even in high sulfur concentrations. Thus lifetime of aerosols in SALSA is reduced due to the more efficient removal when injected to higher latitudes compared to *Baseline*. In M7, there is not large difference in lifetime of aerosols between *Baseline* and *Wide* scenarios. Overall, the global mean total (SW+LW) radiative forcing was roughly 20% larger than
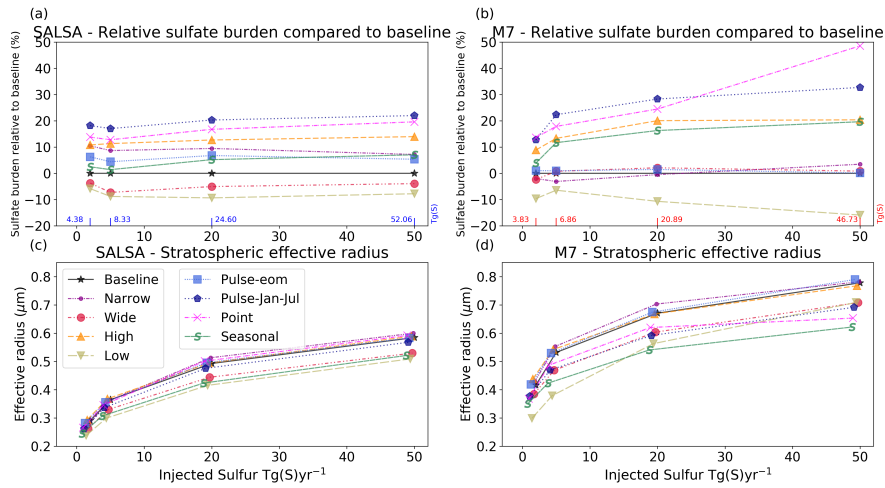
Figure 7. a-b) Relative stratospheric sulfur burden in sensitivity scenarios compared to *Baseline* scenario with corresponding sulfur injection rate. c-d) Global mean effective radius of stratospheric aerosols

450 in the *Baseline* scenario when simulated with M7 while with SALSA, the difference was between ±4% depending on the injection rate.

Wider injection area decreases the radiative forcing over the tropics while increasing it at higher latitudes compared to *Baseline* scenario (Fig. 8). However, the difference in radiative forcings at the tropics with 50 Tg(S)yr^{-1} injection rate between scenarios *Baseline* and *Wide* was rather small in M7(<10%). In the *Baseline* scenario, higher injection concentration due to the

455 narrower injection area (10° N - 10° S) enhances the effective radius of stratospheric particles in M7 to be larger than 0.8 μm which is not an optimal size for scattering radiation (Fig. 9).

As expected, a narrower injection area (two model grid boxes over the Equator) (*Narrow*-scenario) led to larger effective radii of stratospheric aerosols in both models compared to the *Baseline* scenario. However, sulfur lifetime increases as sulfur is injected into stratospheric tropical pipe~~where uplifting is even further increased due to heating of the atmosphere caused by~~

460 ~~aerosols (see sect. 3.4)~~. As in the case of scenario *Wide*, the impact of the locally larger injection rate does not increase effective radii of aerosols in SALSA as much as in M7 and the lifetime of particles was 10% longer in scenario *Narrow* than in scenario *Baseline* due to the impact of atmospheric circulation. Thus, the radiative forcing of injection scenario *Narrow* was larger than in the *Baseline* scenario and it decreased gradually from 23% to 8% when the magnitude of sulfur injections was increased from 2 to 50 Tg(S)/yr, based on SALSA simulations. Simulations with M7 show that the *Narrow* injection strategy does not

465 affect significantly the lifetime of aerosols and the net radiative forcing in the *Narrow* scenario was of the same magnitude or slightly lower than in the *Baseline* scenario in M7.
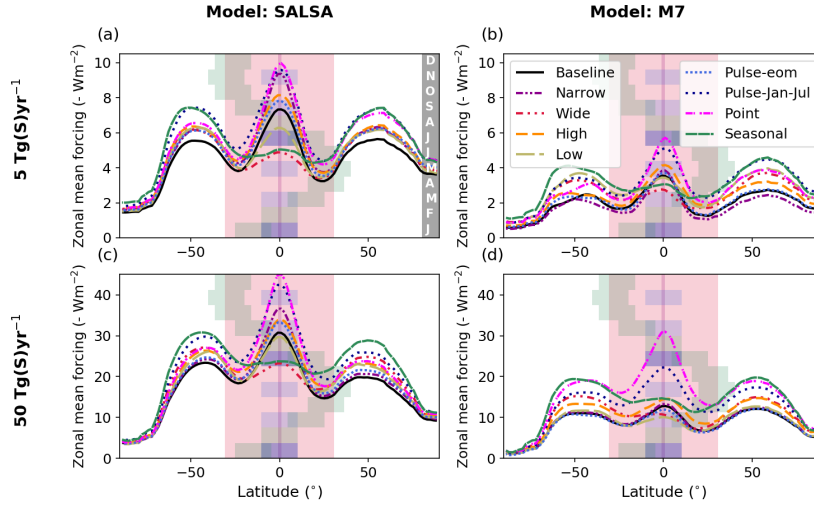
Figure 8. Zonal mean clear sky net forcing with a-b) 5 and c-d) 50 Tg(S)yr^{-1} injection rates in simulated sensitivity scenarios. SALSA results are shown in the left and M7 results on the right panels. Note that y-axes scale shows negative (cooling) values. Shaded areas show latitudes of injection area at the time of year (y-axes, month shown in right edge of panel a)) in each injection scenario. Latitudes of injection area are same in *Baseline*, *High* and *Low* scenario (10° N - 10° S).

3.3.2 Injecting to one grid box instead of a band over longitudes

In scenario ~~Onegb~~*Point*, the injection area in *Narrow* was shrunk also in the meridional direction, reducing it to one gridbox. This further increased sulfur injection rate in the injection area as sulfur injections are concentrated on the smaller region.

470   However, as ~~sulfur is injected longitudinally to~~ injection takes place longitudinally in an area which is ~~only one model~~ one grid box wide, ~~less~~ existing aerosols over the Equator ~~are under continuous injection~~ from previous injections are not, most of the time, condensation and coagulation sink for injected sulfur in the injection area, as is the case when injections occur across all longitudes. Even though sulfur is mixing relatively fast over longitudes, the available gaseous sulfate for condensation or nucleation is localized nearby the injection area in the ~~Onegb~~*Point* scenario.

475   Based on simulations with SALSA, scenario ~~Onegb~~*Point* was the second most efficient of the studied SAI strategy, regardless of the magnitude of injections. The mean net clear-sky radiative forcing in the ~~Onegb~~*Point* scenario was 23-32% larger than in the *Baseline* scenario, depending on the injection rate. Results of the ~~Onegb~~*Point* scenario with M7 showed significantly different behaviour when increasing the injection rate compared to the other scenarios and even ~~in~~ to the same scenario ~~using SALSA .~~ when SALSA was used instead of M7: While the clear sky global mean net radiative forcing was roughly 40% larger

480 compared to the *Baseline* scenario with injection rate of 2, 5 and 20 Tg(S)y^{-1}, it was 91% larger in the case of injection rate of 50 Tg(S)y^{-1}. To study this in more detail, additional simulations of ~~Onegb~~*Point* injection scenario were simulated with M7 and with 10, 30, 40, 70 and 100 Tg(S)y^{-1} injection rates. The ~~Global~~global mean SW radiative forcing, forcing efficiency, and the lifetime and effective radius of stratospheric aerosols from these simulations are shown in Fig. ~~S4~~ S6 in the supplement. All
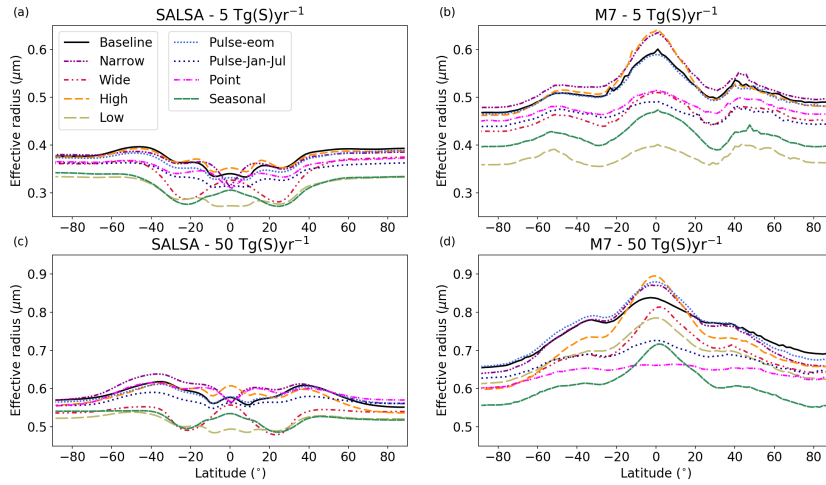
Figure 9. Zonal mean effective radius of stratospheric aerosols in studied sensitivity scenarios for 5 (a and b) and 50 (c and d) Tg(S)yr^{-1} injection rates simulated with SALSA (left panels) and M7 (right panels).

simulations with SALSA and all other scenarios with M7 were showing the following: the effective radius increases and the
485 SW radiative forcing efficiency and lifetime of aerosols decrease with an increasing injection rate. However in the ~~Onegb~~ _Point_ scenario with M7, the lifetime of aerosols increased with increasing injection rate when injection rates were larger than 20 Tg(S)y^{-1}. In addition, SW forcing efficiency did not ~~decreased~~ decrease and the effective radius of stratospheric aerosols did not ~~increased similarly~~ increase gradually with the injection rate as in simulations with SALSA and ~~all other scenarios when the injection rate was increased from 20 Tg(S)y^{-1}~~ in all the other scenarios.

490   A closer look at the aerosol number size distributions over the Equator in _Baseline_ and ~~Onegb~~ _Point_ scenarios shows why the lifetime and SW radiative forcing increased in ~~Onegb~~ _Point_ scenario with increasing injection rate (Fig. ~~S5~~S6). In the _Baseline_ scenario, number concentration of accumulation size aerosols decreased whereas number and size range of coarse mode increased with increasing injection rate. This did not happened in ~~Onegb~~ _Point_ scenario, where the number of accumulation ~~model~~ mode sized aerosols increased and median radius of coarse mode did not ~~growth~~ grow the same way as in _Baseline_ scenario. In
495 addition, when the injection rate exceeded 30 Tg(S)$^{-1}$, the coarse mode shrank with increasing injection rates, which probably explains the increase in the mean lifetime of aerosols. This also contradicts the results of Niemeier and Timmreck (2015) where ~~injection to the~~ the size of the coarse mode increased with the injection rate in a simulation of injections to one grid box~~were simulated~~.

    It is not totally clear what is causing this peculiar behaviour in this one scenario and only when simulated with M7. The
500 scenario, where sulfur is injected to a single grid box, differs from all others in two ways 1) the concentration of injected SO$_2$ is significantly higher compared to scenarios with injections over a whole latitude band and as was pointed out earlier, this also may lead to a OH limitation for sulfate formation, which is however not simulated with prescribed chemistry, 2) in the

OnegbPoint scenario, aerosols over the Equator are not ~~under~~ experience continuous injections except in one model grid box. Inside the injection area concentration of nucleation particles is high and these particles can grow to the size range of Aitken mode by self-coagulation and condensation. This is seen as larger number concentration at the longitude where injections take place (Fig. ~~S6b~~S8b). If compared for example to the size distribution of *Baseline* scenario (Fig. 2), the number concentration of Aitken mode aerosols is significantly larger and thus it can also compete more efficiently with coarse mode for available sulfate gas. This results in also larger number of accumulation mode aerosols than in *Baseline* scenario and thus also larger SW radiative forcing. On the other hand, the size of the coarse mode particles is significantly smaller in ~~Onegb~~*Point* than in *Baseline* scenario. The mean radius of the coarse mode is affected by several processes: coagulation and condensation on the coarse mode aerosols are increasing the size of the coarse mode, while sedimentation and reallocation of aerosols from accumulation mode to coarse mode decreases the mean radius. It seems that with a high enough injection rate (more than 30 Tg(S)yr~~−1~~$^{-1}$) the processes contributing to the shrinking of the mode are more efficient resulting in an overall decrease in the size of the coarse mode. In addition, coarse mode particles, which are carried around Equator, are ~~under~~experienced continuous injections in *Baseline* scenario and growth to larger size through the efficient condensation and they also coagulate efficiently with the formed new particles. In ~~Onegb~~*Point* scenario this is not happen as there is significantly less available H_2SO_4 outside of injection area (Fig. ~~S6a~~S8a).

As was mentioned, this peculiar behaviour was not seen in Niemeier and Timmreck (2015) where similar scenario was simulated with the M7 in earlier generation of ECHAM. However, as the atmospheric model, background conditions (e.g surface aerosol emissions) and resolution were different than here, this peculiar behaviour might be somehow related also atmospheric dynamics ~~. This is supported the fact, that in this study *Onegb* scenario was first simulated with the untuned model version and these peculiar results in *Onegb* were not seen in those simulations. Overall this~~ (Niemeier and Schmidt, 2017). It indicates that this unique behaviour seen in the lifetime of aerosols and radiative forcing in ~~Onegb~~*Point* scenario is probably caused by nonlinearities in the microphysical processes and dynamical changes and restriction of modes in aerosol size distribution in M7. This shows that simulating extreme cases, where sulfur concentration is locally large, might lead to peculiar behaviour of a modal model. This should be kept in mind also when simulating e.g supervolcanoes. In any case, together with the significant difference in model responses seen between M7 and SALSA on the SAI, these peculiar results in ~~Onegb~~*Point* highlight need for better tools or observational data to evaluate models.

Zonally, scenario ~~Onegb~~*Point* led to the largest radiative forcing at the Equator out of all studied scenarios in both models. Most notably, ~~Onegb~~*Point* stands out in simulations of 50 Tg(S)yr^{-1} injection rate with M7, where radiative forcing is ~~240~~230% larger over tropics than in *Baseline* scenario. In addition, radiative forcing over the tropics in the ~~Onegb~~*Point* scenario with M7 was close to the results of the *Baseline* scenario with SALSA even though simulations with SALSA generally showed much larger radiative forcing. Several studies have shown that offsetting GHG induced global average warming by SRM lead to cooling at the tropics while high latitudes are warmer in case of equatorial injection or in an idealized case, where SRM is imitated by reducing the solar constant (Aswathy et al. (2015), Jones et al. (2016), Kravitz et al. (2016), McCusker et al. (01 May. 2012) and Yu et al. (2015)). Even though injecting sulfur to one gridbox turned out to be an efficient injection strategy in the simulations of both models, the cooling is strongly concentrated over the tropics. The ~~Onegb~~*Point* injection strategy might

make the fundamental problem of SRM, where tropics is cooled more at the expense of cooling of high latitudes, worse, if injections are concentrated in the tropics.

3.3.3 Sensitivity to injection altitude

Several studies have shown that the lifetime and the radiative forcing of stratospheric aerosols increase with the altitude of injections due to a longer sedimentation path (Heckendorn et al. (2009); Niemeier et al. (2011); Kleinschmitt et al. (2018); Vattioni et al. (2019); Tilmes et al. (2018b)). Here we studied the impact of injection altitude using three scenarios, *Low*, *Baseline* and *High* scenarios, where sulfur is injected to 18-20 km, 20-22 km and 22-24 km altitudes, respectively. When compering scenario *High* to the *Baseline* scenario, our results with both models were consistent with the earlier studies. The injection rate did not have a large impact on how radiative forcing of sulfur injection to high altitudes compares with results of our *Baseline* scenario. Injecting sulfur to a higher altitude led to 14-16 % larger net radiative forcing compared to the *Baseline* scenario when simulated with SALSA. With M7, scenario *High* led to 7-15% larger net radiative forcing than the *Baseline* scenario. As Fig. 7 shows, the injection to higher altitude led to effective radii values close to results of the *Baseline* injections while stratospheric sulfate burden was 12-20% larger in simulations with both models. This indicates that the larger radiative forcing in injection scenario *High* is caused mainly by a longer sedimentation path and the size distribution of aerosols is not significantly affected by the differences in the microphysical processes due to the injection altitude.

The Our results indicate that the impact of atmosphere dynamics on aerosol microphysics had a clearly larger role when injecting to lower altitude (18-20 instead of 20-22 km in *Baseline*). While the lifetime of aerosols was reduced as expected (Fig. 7a,b) because of the shorter sedimentation path, effective radii were also clearly smaller than in the *Baseline* scenario. This is consistent between the microphysical models. Simulations with SALSA showed that injecting sulfur to lower altitude enhanced net clear sky radiative forcing by 2-6% compared to radiative forcing in the *Baseline* scenario. In M7, the radiative forcing was 14-21% larger than in the *Baseline* scenario in the case of injection rate of 2-20 Tg(S)yr^{-1}, but 50 Tg(S)yr^{-1} injection rate led to roughly the same global mean radiative forcing as in the *Baseline* scenario.

Smaller aerosols in scenario *Low* compared to *Baseline* originated from differences in the atmospheric circulation at the different altitude. Fig. S7 S9 in supplement shows the average meridional wind speed in the scenario *Low* with 5 Tg(S)yr^{-1} injection rates simulated with M7. In *Low* scenario, when injecting to lower altitude (18-20km), mean wind patterns point from the Equator to higher latitudes. Winds are carrying more aerosols from Equator to high latitudes which reduces the sulfur concentration over the Equator compared to the *Baseline* scenario. This conclusion can be drawn also by analyzing where SO$_2$ is oxidized to sulfate. In the case of 5 Tg(S)yr^{-1} with M7 shows that 10-30% less sulfate is produced via SO$_2$+OH over the Equator in the *Low* scenario than in the *Baseline* while in the subtropics and mid latitudes sulfate production is 10-50% larger (supplement Fig. S7S9). As there is less H$_2$SO$_4$ gas over the Equator to condensate on the existing particles, particles are smaller in *Low* scenario than in the *Baseline* scenario. Also due to the atmospheric circulation which carries more efficiently aerosols to higher latitudes, the zonal radiative forcing is concentrated more on midlatitudes than the tropics in case of injections to the lower altitude compared to the *Baseline* scenario Fig. 8.

Our conclusions on the sensitivity of the radiative forcing to the injection altitude differ from the conclusions of Niemeier and Schmidt (2017). Their study showed that injecting sulfur to the altitude of 60 hPa (19km) resulted in a larger radiative forcing than injecting sulfur to 30 hPa (25km), when the injection rates were larger than 10 Tg(S)$^{-1}$. Here in our simulations, scenario *Low* led to a larger radiative forcing compared to the injections to the altitude (20-22km) used in the *Baseline* scenario

575 also in case of smaller than 10 Tg(S)$^{-1}$ injection rate. In addition, in the case of 50 Tg(S)$^{-1}$ injection rate simulated with M7, model results did not show a large difference in the global mean radiative forcing between scenarios *Low* and *Baseline*. When comparing to our scenario *High* (22-24km), which is close to higher altitude studied in Niemeier and Schmidt (2017), the radiative forcing from *Low* injection strategy was higher only in the case of 5 Tg(S)$^{-1}$ injection rate simulated with M7. However in Niemeier and Schmidt (2017) sulfur were injected to one grid box while here sulfur were injected band over the

580 longitudes and different model version and resolution was used. Overall this means that universal conclusion how injection altitude affects direct aerosol radiative forcing cannot be drawn as the results are depending on the atmospheric circulation in the altitude where injections take place, as well as injection rate and width of the injection area.

3.3.4   Sensitivity to temporal variation of injections

In addition to scenarios where sulfur was injected continuously over a year, we studied two scenarios where the injections

585 were concentrated only to a certain time of year. In scenario ~~Pulse2m~~*Pulse-eom*, injections were done during every second month starting from January and in ~~Pulse6m~~*Pulse-Jan-Jul* injections were done in one month long periods twice per year, in January and July. Results from the ~~Pulse2m~~*Pulse-eom* scenario were close to results of the *Baseline* injection strategy in both models. One month frequency between suspending injection and restarting it, is relatively short compared to the time required for transportation, oxidation or growth of the particles to have a significant impact on results compared to continuous

590 injections over the year. Some of the aerosols moved out from the injection area during the pause in injections, which decreased condensation and coagulation on the existing particles over the Equator compared to the *Baseline* scenario. However, in the ~~Pulse2m~~*Pulse-eom* scenario injection rate at the time of the injection is doubled. In SALSA, the latter does not decrease radiative forcing efficiency as much as in M7 due to more efficient nucleation at the expense of condensation. Thus, in SALSA simulations, the lifetime of aerosols was roughly 5 % longer and the global mean radiative forcing was 10-15% larger in

595 ~~Pulse2m~~*Pulse-eom* than in the *Baseline* scenario. Simulation with M7 did not show a significant difference in the global mean radiative forcing between scenarios *Baseline* and ~~Pulse2m~~*Pulse-eom* (-3 - 7%).

In the ~~Pulse6m~~*Pulse-Jan-Jul* scenario, the amount of injected SO$_2$ was ~~5~~ 6 times larger during the injections compared to continuous injections. However, there was a 5 month period where the injections were suspended and aerosols had time to transfer to higher latitudes, before the next injection period was started. Thus, when a new injection period started, there

600 were less particles ~~present at the injection are~~ from the preceding ~~injection where injected sulfur could condensate or where new nucleated particle could coagulate with~~injections present over the Equator. Thus, condensation on existing particles and coagulation between the new and old particles are lower than in case of continuous injections. This reduces particles average size compared to *Baseline* injections. The zonal effective radius was smaller in all latitudes compared to the *Baseline* scenario in both models and all injection magnitudes (see Fig. 9). This enhanced the lifetime of aerosols by 17-35% with M7 and 20-

605 27 % with SALSA. Based on SALSA simulations, the forcing efficiency of the ~~Pulse6m~~Pulse-Jan-Jul scenario were largest of all studied scenarios as the forcing was over 30 % larger than in the *Baseline* scenario. The results of M7 show even a larger radiative forcing of the ~~Pulse6m~~Pulse-Jan-Jul scenario compared to *Baseline* and its relative radiative forcing increased gradually from 40% to 58% when the injection rate was increased from 2 to 50 Tg(S)/yr.

It is expected that the results of the scenario, where sulfur is injected only during certain months, are sensitive to which
610 months injections take place and how long the injection periods are. Atmospheric circulation varies during the year and the transportation and also the growth of aerosols are dependent on the timing of the injections. In addition, the seasonal cycle of solar radiation and how it coincides of the aerosol field has a large impact on the efficiency of SAI as well as the available OH for oxidation of SO_2. As shown by Visioni et al. (2019), radiative forcing is significantly dependent on the season, when injections takes place.

615 ### 3.3.5 Seasonally changing injection area

Last of the studied scenarios was one where ~~injections are varied seasonally, as suggested by Laakso et al. (2017). The aim of this type of~~ a 20° wide injection area is varied gradually between 40° N and 40° S during the year. As suggested in Laakso et al. (2017), the aim of seasonally changing strategy is to increase the efficiency of SAI compared to continuous Equatorial injections by targeting aerosol fields to coincide with maximum solar radiation during the year and reducing the
620 particle size by varying the injection area so that sulfur is not always injected to regions where there are pre-existing larger aerosols from preceding injections. Another objective is to produce relatively less cooling in the tropics and more on mid and high latitudes compared to continuous Equatorial injections. This could prevent the over cooling of the tropics and under cooling of polar regions in the case of where average GHG-induced warming is offset by Equatorial injections (Laakso et al. (2017)).

625 Figure 6 shows that based on SALSA simulations, the global mean clear sky radiative forcing of scenario *Seasonal* was 10-20% larger compared to ~~Equatorial injections~~*Baseline* scenario. Simulations with M7 showed also a significant enhancement in the global mean radiative forcing especially with injection rates higher than 5 $Tg(S)^{-1}$ for which the radiative forcing was 45-57% larger than in the *Baseline* scenario. The size of the stratospheric aerosol was also smaller as Fig. 7 shows that the effective radius of stratospheric aerosols in the case of seasonal injections was clearly smaller compared to Equatorial injections. Further,
630 Fig. 8 shows that the clear sky zonal mean radiative forcing was concentrated in the mid-latitudes rather than over the tropics. ~~The results of the~~ Here the variation of the injection area between latitudes in *Seasonal* ~~injection strategy was shown to be~~ scenario were implemented so that the northmost position(40° N - 20° N) takes place at the May. The results of seasonal injection strategy are sensitive to the phase ~~in which the injection regime was varied i.e if injection area has north-/south most position in boreal summer~~when the north/~~winter Laakso et al. (2017)~~southmost position occurs. This affects the probability of
635 optimal size particles coinciding with maximum incoming solar radiation, how fast SO_2 is oxidized, and also how aerosols are transported in the atmosphere because OH concentration and atmospheric circulation varies during the year. Different phases of seasonally varying injection are in the case of 5 $Tg(S)yr^{-1}$ was studied with ECHAM-HAMMOZ with SALSA in Laakso et al. (2017). ~~In that study, none~~None of the studied seasonally varying injection strategies in Laakso et al. (2017) led to a

higher than 3% global mean radiative forcing compared to Equatorial injections, ~~while in our current study the~~ . However in this study the simulations of seasonal injection with 5 Tg(S)yr^{-1} ~~lead to~~ and with SALSA led to a 10 % ~~larger radiative forcing . However, there~~ stronger radiative forcing compared to *Baseline* scenario. There are several differences between the simulations here and simulations done in Laakso et al. (2017). The vertical resolution of in the model simulations in Laakso et al. (2017) was 47 levels which is not enough to reproduce the QBO ~~(here 95 vertical levels were used)~~. Injection strategies were slightly different e.g sulfur were injected at 20km of height (here 20-22km); in most cases injection regime varied between 30° N and 30° S (here 40° N and 40° S); here the northern-most position of the injection regime is reached in May, while in Laakso et al. (2017) studied scenarios where north-most position were April and June. In addition, here a newer version of ECHAM-HAMMOZ is used.

3.4   Dynamical changes in the stratosphere and effects on the quasi-biennial oscillation

As previous sections has concentrated mainly aerosol microphysics and its impact on lifetime of aerosols radiative forcing here we study shortly changes in atmospheric dynamics. Stratospheric aerosol fields absorbs radiation which in turn warms the stratosphere. When sulfur was injected in the stratosphere, the warming it induced was strongest in the latitudes where the aerosol fields were located (Fig. 10). Increasing the magnitude of injections led to stronger warming in the stratosphere and the temperature anomalies were significantly higher in M7 than SALSA as expected based on the amount absorbed LW radiation (Fig. 1). Based on SALSA, warming anomalies inside the injection regime (10° N - 10° S, 20-22 km altitude) were 0.39, 1.07, 3.26 and 6.83 K for 2, 5, 20 and 50 Tg(S)yr^{-1} injection rates respectively while the corresponding temperature anomalies were 1.04, 2.28, 6.84 and 11.48 K in M7 simulations.

Stratospheric warming was concentrated in the tropics in all studied SAI scenarios, but the magnitude of warming depended on the injection strategy (see supplement Fig. ~~S8-9~~ S10-11). Injecting sulfur to a narrow band over the Equator (*Narrow*-scenario) led to a stronger stratospheric warming than seen in the *Baseline* scenario, while in scenario *Wide* there was less warming. As expected, varying the injection area seasonally (~~Seasonal~~*Seasonal*) did not warm stratosphere as much as the other scenarios.

As the tropical stratosphere warms, it changes the dynamics of the atmosphere: for instance, it leads to a stronger vertical advection which further strengthens the lofting of aerosols and makes the lifetime of aerosols longer. Figure 11 shows the residual vertical velocity (ω^*) between 10° N - 10° S latitudes in baseline scenarios with the different injection rates. Higher injection rate causes stronger warming which further strengthens ω^* at the injection altitude (20-22 km) and even up to 30 km altitude. As expected, based on the stronger warming seen in M7 than SALSA (Fig. 10), the increase in the updraft velocity is generally higher in M7. In case of the 100 Tg(S)yr~~-1~~$^{-1}$ in injection rate in M7, at the 20km altitude the increase in ω^* was 360 %. However, note that the profiles of ω^* in the CTRL simulation without SAI were significantly different between SALSA and M7. This is discussed later in this section. While residual vertical velocity increases above tropopause, in the upper troposphere the residual vertical velocity decreases with the simulated injection rate. This reduction is larger in M7 than SALSA and simulation of 100 Tg(S)yr^{-1} injection rate with M7 showed 35% lower residual vertical velocity at 15 km altitude compared to CTRL simulation. One interesting feature is also seen in altitudes higher than 25 km, where the ω^* changes
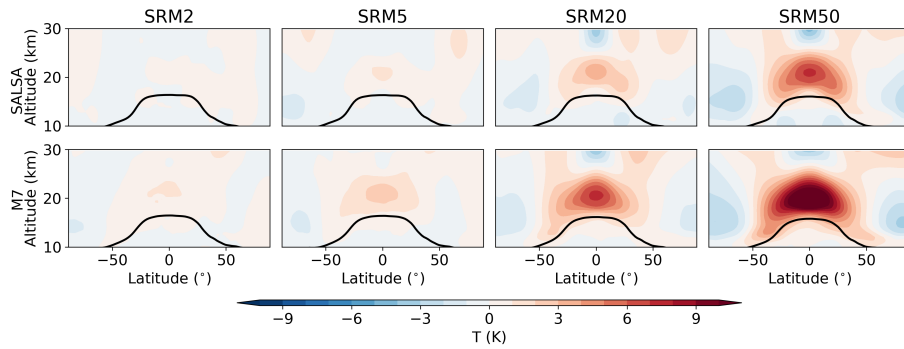
Figure 10. Temperature anomaly due to the *Baseline* stratospheric sulfur injection with different injection rates simulated with SALSA (upper panels) and M7 (lower panels). Black line indicates tropopause.
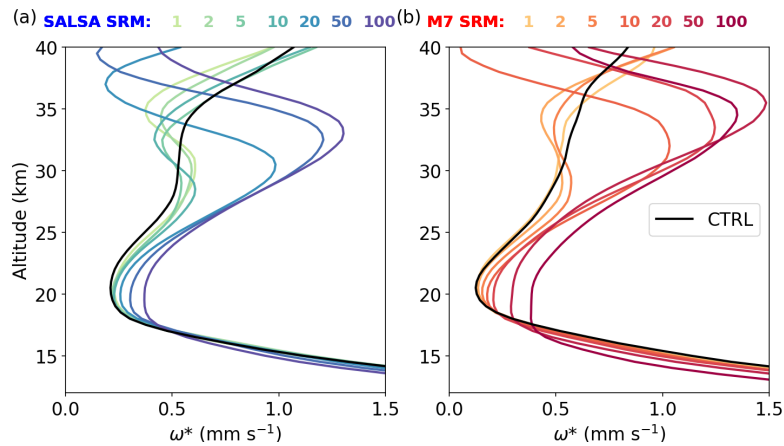
Figure 11. Residual vertical velocity in the tropics ($10°$ N - $10°$ S latitudes) for different injection rates in simulations with a) SALSA and b) M7

drastically when the injection rate is large enough. In SALSA, this takes place in injection scenarios higher than 10 Tg(S)yr~~−1~~$^{-1}$ while in M7 this happens already with injections higher than 5 Tg(S)yr~~−1~~$^{-1}$. While in lower than above-mentioned injection

675 rate, ω^* is roughly 0.5 mms~~−1~~$^{-1}$ at the 30km altitude, in case of larger injection rate ω^* is larger than 1.0 mms~~−1~~$^{-1}$. Tropical ω^* in different injection scenarios compared to baseline scenario with injection rates 5 and 50 Tg(S)yr~~−1~~$^{-1}$ are shown in supplement Fig. ~~S10~~S12.

Changes in zonal and meridional wind patterns in December-January-February and June-July-August are shown in the supplement (Fig. ~~S11-14~~S13-16). Zonal wind increase in the tropics is stronger with higher injection rates and in M7 than in

680 SALSA. The meridional wind pattern anomalies in SAI scenarios have in some cases different signs between SALSA and M7. Stratospheric sulfur injections have also been shown to e.g strengthen the stratospheric polar vortex Visioni et al. (2020a). It

is expected that these changes are also sensitive to the aerosol model as well as to the injection strategies. However, a more detailed analysis of this is beyond of the scope of this study.

One consequence of the warming of the tropical stratosphere in case of equatorial injections is the slowing down of the quasi-biennial oscillation (QBO) and if the injection rate is high enough, the QBO can be shut down completely ((Niemeier and Schmidt, 2017))(Niemeier and Schmidt, 2017). This statement was supported also by our simulations. As can be seen in Fig. 12, the QBO was slowing down with increasing injection rates. Based on M7 simulations, the shutting down of QBO takes place for injection rates higher than 10 Tg(S)/yr while in SALSA more than 20 Tg(S)yr^{-1} is required. This corresponds to stratospheric temperature anomalies compared to the CTRL scenario, which were the same magnitude in those two simulations. In addition, after the shutting down of the QBO, the westerly phase of QBO in the lower stratosphere is stronger and it reaches higher altitudes in M7 compared to results of the corresponding injection magnitude in SALSA. In M7, stratospheric heating due to stratospheric aerosols was stronger than in SALSA and thus the QBO slows down and vanishes with lower injection rates. A similar difference in the impacts on the QBO between climate models has been seen in Niemeier et al. (2020) which were caused difference in residual vertical velocity between models and different heating rates in the lower stratosphere. Probably also here, difference in responses in QBO between models are not fully caused by aerosol microphysics.

As Fig. 11 and Fig. 12 show, residual vertical velocity and QBO were different between the aerosol schemes initially even without the stratospheric sulfur injections, even though the same atmospheric model was used. In the CTRL simulations, M7 has a much longer period of QBO than in SALSA and it is overestimated compared to 28 months seen in observations (Naujokat (1986)). Even though the same atmospheric model was used, different tuning parameters are used depending on the aerosol microphysical model and the atmospheric temperature is not consistent between models even in CTRL simulation (supplement Fig. S15S17). Based on test simulations, which were performed before the actual simulations of this study, the tuning of the model had a significant impact on the QBO. In addition, even though aerosol concentration in the stratosphere is low in CTRL simulations, the tropospheric aerosols and the following indirect cloud impacts are different between the aerosol schemes used. In M7 simulations, modes were modified to represent stratospheric aerosols more accurately by narrowing the standard deviation of the coarse mode and changing the threshold radius when aerosols from the accumulation mode are transferred to the coarse mode. A disadvantage in this modified setup is that large tropospheric aerosols are probably not represented as well as in the standard setup. Differences in tropospheric aerosols and tuning parameter led to warmer upper troposphere and lower stratosphere in SALSA than in M7 as seen in supplement Fig. S15S17. Thus residual vertical wind (Fig. 11), zonal and meridional wind patterns and QBO in CTRL simulations are different between SALSA and M7. This also will lead some bias in atmospheric circulation in the studied SAI scenarios between the models.

Franke et al. (2021) and Kravitz et al. (2019) have shown that the response of the QBO to sulfur injections depends on the location of injections. In Franke et al. (2021) simulation where sulfur was injected to two gridboxes located at 30° N and 30° S and in Kravitz et al. (2019) were sulfur was injected to 4 different latitudes based on a feedback algorithm, the QBO was not significantly affected even with 25 Tg(S)$^{-1}$ injections. QBO in our sensitivity scenarios is shown in the supplement (Fig. S13S18). Studied scenarios here included injections at the Equator. However, in scenario Seasonal, the injection region varied and sulfur was injected to Equator only during a part of the year. In this case, sulfur injection did not have a significant impact
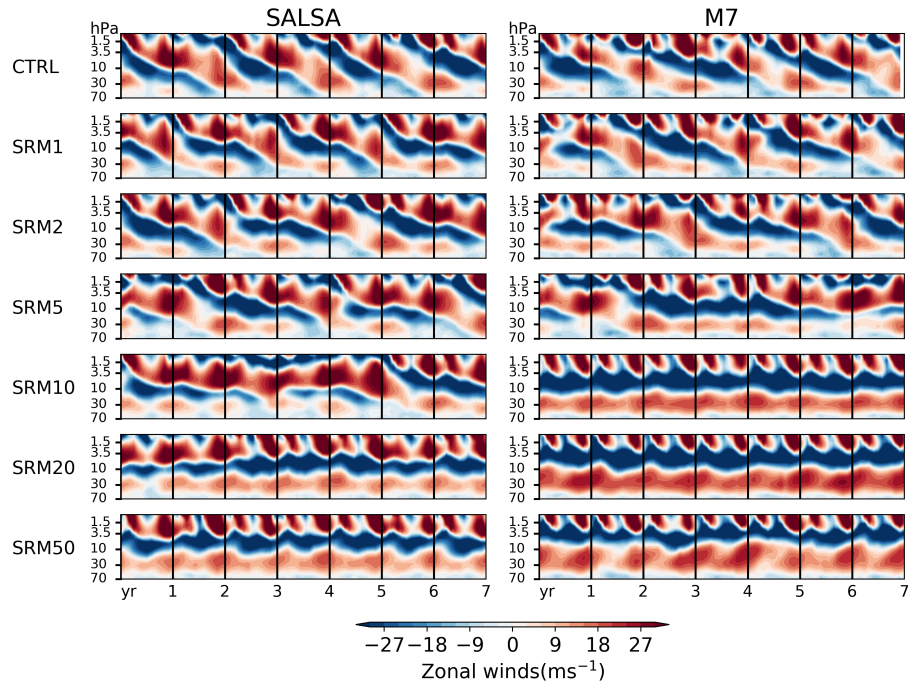
Figure 12. Zonal mean zonal wind (ms^{-1}) at the Equator for CTRL and stratospheric sulfur injection with different injection rates. SALSA results are shown in left panels and M7 results are in right panels

on QBO even if 50 Tg(S)$^{-1}$ were injected in SALSA simulation. The results of the corresponding scenario with M7 showed that QBO was prolonged with 20 Tg(S)$^{-1}$ and shut down with 50 Tg(S)$^{-1}$ injection rates. In all the other scenarios, the QBO vanished with 50 Tg(S)$^{-1}$ injection rate and in most scenarios with an injection rate of 20 Tg(S)$^{-1}$ in both models. In *Low*,

720 *High* and *Wide* scenarios QBO did not fully disappear in the case of 20 Tg(S)$^{-1}$ injection rate with SALSA, but the cycle were significantly prolonged.

4 Conclusions and discussion

Here we have systematically studied different spatio-temporal injection strategies with different magnitudes (2-100 Tg(S)yr^{-1}) of sulfur injections using both the sectional (SALSA) and modal (M7) aerosol schemes in ECHAM-HAMMOZ. These simu-

725 lations showed significant differences in SW and LW radiative forcings, size of the aerosols and lifetime of sulfur between the different injection strategies. In addition, modelled results were very sensitive to which microphysics model was used in the simulations. While both models show sublinear increase of the global mean net radiative forcing as a function of the amount of injected sulfur due to the increases in the size of aerosols, the net radiative forcing of SAI was 88-154% higher based on simulation with SALSA than M7. This large difference was also present when SW and LW radiative responses between

730 models were compared individually. While SW radiative forcing was 45-85% higher (more negative) in SALSA than M7 with corresponding injection rate, LW radiative forcing was 33-67% larger in M7.

We identified two main factors which were causing different responses between models: 1) The numerical methods for describing the competitive processes of new particle formation and condensation inside the injection regime and 2) ~~limiting the evolution and the shape of the particle size distribution due to mode setup in M7~~ a local minimum in aerosol number size
735 distribution between two largest modes, caused by repartitioning of particles between the modes in model, which coincidences with the optimal particle size for backscattering. In the stratosphere, new particle formation by nucleation is fed by continuous injections. On the other hand, there are already pre-existing particles from the preceding injections to which injected sulfur can ~~condensate~~ condense. Thus, there is a competition between these two processes for available sulfuric acid gas. In SALSA, ~~the nucleation rates are higher than in M7 and sulfuric acid gas~~ sulfuric acid tends to form new particles rather than condensing
740 on the ~~existing ones . In~~ pre-existing ones while in M7 simulations the opposite is true~~, and sulfate tends to condense on pre-existing particles and leave less sulfur available for nucleation~~. Simulations with M7 showed that continuous injections and condensation increased the size of the largest (coarse) mode. However due to the setup for the repartition of particles between modes, this did not allow the second largest mode to grow, creating a gap in the particle size distribution between the two largest modes. This gap coincided with the particle size range which would be optimal to scatter radiation.

745 There are several factors which support a sectional model over a modal model for stratospheric aerosol simulations, despite the fact that the modal scheme is significantly computational faster than sectional (simulations with M7 were 60% faster than SALSA). First of all, tropospheric and stratospheric aerosols require different configurations for modes and thus studying both in the same simulations is not recommended. In addition, even though only stratospheric aerosols are studied, the tropospheric aerosols, which were not well represented by configuration designed for stratospheric aerosols, can affect indirectly to stratospheric
750 aerosols. In SAI simulations, and especially in the case of continuous injections, the size distribution inside the injection region does not have a clear multimodal structure in the sectional model simulations except for the lowest injection rates (1-2 $Tg(S)yr^{-1}$) (Fig5 and FigA3) (English et al. (2012), Kleinschmitt et al. (2018)). This is probably because there is available H_2SO_4 gas for particles to grow by condensation, and particles are not accumulating to certain size classes by coagulation. This kind of size distribution cannot be represented by 4 modes and in this study the problem culminates in that there is a
755 persistent gap between the two largest modes. One option could be to use more modes, but then the computational benefits compared to sectional schemes would become smaller. In the standard setup of M7 (the largest) coarse mode width is 2.0 instead of 1.2 which is used here. This would make the gap between the two largest modes smaller. However in the case of stratospheric sulfur injections or a large volcanic eruption, a wider coarse mode width leads to a tail of large particles. This causes an overestimation of the effective radius of the coarse mode and increased the sedimentation velocity and reduced
760 residence time of aerosols in the stratosphere which is the reason why the different setup is used for stratospheric aerosols. One option could be to increase mode widths of the Aitken and accumulation modes. However, number concentrations of these modes are typically higher and thus widening of the modes can lead to a situation, where widened mode would cover the adjacent larger mode. It is also good to keep in mind that the partitioning of sulfuric acid to particle phase due to nucleation over condensation was suspiciously large in SALSA and the model produced significantly larger net total radiative forcing than

765 in e.g. Kleinschmitt et, al. (2018), where simulations were done with the sectional model. Thus, even though there was not as clear a shortcoming as the gap between modes in M7, there is a need to analyze the individual microphysical processes and to understand the differences between the results of different sectional models.

Overall, differences in the results between the two microphysical models reveal significant uncertainties related to stratospheric sulfur injections. Thus, there is a need for better tools to analyze aerosol microphysical processes in stratospheric 770 conditions under continuous injections and to improve the aerosol-climate models. A comparison with the observations of large volcanic eruptions (e.g Pinatubo) does not necessarily offer a true picture of the model performance under continuous injections as there is not as large competition in nucleation and condensation in the case of volcanic eruptions, where a large amount of sulfate erupts abruptly to a relatively particle free stratosphere. It is also good to keep in mind that sulfur would most plausibly be injected to the stratosphere by aircraft (Smith and Wagner (2018)). In these simulations with the climate model 775 the injected SO_2 is instantly mixed in the model grid box with the size of few hundreds square kilometers. Thus microphysics which is taking place inside of plume after injection is not captured by ECHAM-HAMMOZ and aerosol-climate models more in general. In addition, the time step of climate models might be too long for aerosol microphysical processes which can cause strong bias for example here, were sulfuric acid concentrations are high and new particle formation and condensation is resolved simultaneously.

780 ~~Uncertainties~~ Shortcomings and uncertainties in microphysics will further lead to large uncertainties in estimating possible climate impacts of stratospheric sulfur injection or e.g for estimations of how much sulfur is required to achieve a certain climate target. To offer some perspective: compensating all radiative ~~imbalance~~ forcing in the Representative Concentration Pathway (RCP) 2.6 ~~at~~ from preindustrial period to the end of this century ($2.6\,\mathrm{Wm^{-2}}$) by stratospheric sulfur injections would require roughly yearly 3.7 Tg(S) injection based on the results of SALSA while based on M7, 15 Tg(S)yr^{-1} is required to 785 achieve this. The difference is even more significant in extreme cases where the radiation imbalance in the RCP 8.5 scenario ($8.5\mathrm{Wm^{-2}}$) would be compensated by SAI. There, the estimation of required sulfur are either 22 Tg(S)yr^{-1} or over 100 Tg(S)yr^{-1} depending on the microphysical model. These ~~uncertainties between models~~ differences between model results ~~can~~ have also a significant impact on uncertainties related to the global mean precipitation. Larger LW absorption in M7 compared to SALSA might translate to a significant reduction of the global mean precipitation which has been shown to 790 correlate negatively with absorbed radiation Laakso et al. (2020). Lower net radiative forcing in M7 means that more sulfur should be injected to get the same cooling impact as in SALSA, which means even stronger absorption of LW radiation and decrease in the global precipitation. This will be studied further in part 2.

We also simulated different stratospheric sulfur injection strategies with both microphysical models. These scenarios were simulated with 2, 5, 20 and 50 Tg(S)yr^{-1} injection rates. We studied how choices of injecting to narrow vs. wide latitude bands, 795 high vs. low altitude, to one gridbox vs. band over longitudes and temporal differences between injection strategies (pulsed and seasonally changed) affect the radiative forcing of SAI and if the results are consistent between the models.

Differences in all-sky radiative forcing of the most efficient injection strategy compared to the least efficient strategy were 33-42% higher depending on the injection rate based on SALSA. Simulations with M7 showed even larger variation in radiative forcing and all sky radiative forcing in the most efficient SAI scenario was ~~48-216~~ 48-116% higher than in the least

800 efficient simulated scenario. However, ~~if we exclude the~~ simulations of the *OnegbPoint* scenario with ~~50~~ high injection rates (> 20 Tg(S)$^{-1}$ ~~injection rate, which showed spurious results, probably due to numerical issues,~~) simulated with M7 showed an increase in the sulfate lifetime with increased injection rate. This differs from all other scenarios and the *Point* scenario simulated with SALSA. If the Point scenario is not taken into account, in M7 simulations the most efficient SAI scenario exhibited a forcing which was 76% ~~larger than in~~ higher than the least efficient scenario~~based on M7 simulations~~. Based

805 on results from both models, three most efficient scenarios were *Point*, *Pulse-Jan-Jul* and *Seasonal*. Common to all of these scenarios was that instead of a stable injections to band across all longitudes, injections were done either by injecting only to one model grid box, suspending injection for 5 months before the next injection period, or changing injection area seasonally.

Because the forcing efficiency decreases with the injection rate, the injection strategy would matter especially in the case of high injection rate. As an example, based on M7 simulations, in case of 20 Tg(S)$^{-1}$ injection rate, using seasonal injection

810 strategy instead of using Equatorial injections (*Baseline*) would enhance the global mean all-sky radiative forcing by 53%. To achieve the same enhancement using Equatorial injections would require 42 Tg(S)$^{-1}$ injection rate instead of 20 Tg(S)$^{-1}$.

Our *Baseline* scenario, where sulfur was injected continuously between 10° N and 10° S latitudes at 20-22 km altitude resulted in, depending on the injection rate, the smallest or the second smallest net radiative forcings of all studied injection strategies. Only the injection strategy *Narrow* (injecting in a two grid boxes-wide band over the Equator) led to a smaller

815 radiative forcing when simulated with M7 and in the case of 5 and 20 Tg(S)yr^{-1} injection rates. In SALSA, the *Wide* injection scenario was the least efficient when less than 20 Tg(S)yr^{-1} was injected. Based on the simulations, injecting sulfur to lower altitudes (18-20 km) was more efficient than injecting sulfur to 20-22 km altitude in both models with the exception of the simulation with M7 for 50 Tg(S)yr^{-1} injection rate.

If the studied injection strategies are ranked based on their global mean radiative forcing, there are not large differences in the

820 order whether SALSA or M7 results were used. Injecting twice per year, in one-month periods, was the most efficient injection strategy based on SALSA and and M7 with the exception of 50 Tg(S)yr^{-1} when simulated with M7, where the continuous injection to one grid box resulted in a ~~suspiciously~~ exceptionally large impact. Generally, relative differences in the global mean radiative forcings between different the injection strategies were larger when simulated with M7 than SALSA. Overall results from both models indicated that injection over the area where large aerosols from preceding injections already exists

825 would lead to higher condensation on the existing particles, or that new particles will coagulate with the existing ones, which reduces the efficiency of ~~geoengineering~~SAI.

Zonal mean radiative forcings dependence on the injection strategy were qualitatively similar between the models. Equatorial injections in our *Baseline* scenario resulted in maximum zonal forcing over the tropics. This relative disproportion of radiative forcing between low and high latitudes was increased with the higher injection rate. If comparing with the *Baseline* scenario,

830 injecting sulfur to a narrow band or to one model grid box increased the radiative forcing over the tropics, as expected. On the other hand, injecting sulfur to a lower altitude, wider band over the Equator or changing injection area seasonally led to reduced radiative forcing over tropics compared to our *Baseline* scenario. For example, compared to the *Baseline* scenarios, changing injection area seasonally led in SALSA to 29% and in M7 75% larger all sky radiative forcing over non-tropics in case of the injection rate of 5 Tg(S)yr^{-1}. In the Tropics, corresponding changes were 13% smaller and 12% larger with SALSA

835 and M7 respectively. ~~Thus, seasonally varying sulfur injections might prevent~~ Several studies have shown that offsetting the mean GHG-warming with uniform SRM or Equatorial injections can lead to overcooling of the tropics and warming at high latitudes. This ~~has been seen in several studies where GHG-warming has been offset with SRM. This could be done~~ could be prevented by seasonally varying sulfur injections and without any trade off in the total radiative forcing, as net all sky radiative forcing of seasonally changing injection strategy were one of the most efficient of the studied scenarios. Since it also reduced

840 LW absorption compared to the *Baseline* scenario, it would thus lead to smaller reduction in global mean precipitation (Laakso et al. (2020)). ~~In addition, based on~~

We also studied dynamical changes in the stratosphere. As M7 produced larger aerosols and higher absorption of LW radiation, warming in the stratosphere was stronger in M7 than SALSA simulations. Thus the increase in residual vertical velocity was larger and the slowing down of the QBO was more significant in M7 than in simulations with the corresponding

845 injection rate with SALSA. In our *Baseline* scenario the QBO was vanishing with the injection larger than 10 $Tg(S)yr^{-1}$ injection rate based on simulation with M7 while in the simulation with SALSA, more than 20 $Tg(S)yr^{-1}$ was required to shut down QBO. Based on SALSA simulations, the *Seasonal* scenario did not have a significant impact on the slowing down ~~or complete disappearance~~ of the QBO even with 50 $Tg(S)$~~/yr~~ $^{-1}$ injections.

Most of the SAI studies have been focusing on equatorial injections as the baseline case. Injection between 10° N to 10° S

850 was also chosen the injection scenario in G6sulfur GeoMIP experiment ((Kravitz et al., 2015)). As results here show, there are several factors than indicate that equatorial injections should not be used as baseline scenario: 1) It is less efficient than most of the studied alternative injection scenarios, 2) the resulting radiative forcing is concentrated in the tropics and 3) the warming of tropical stratosphere leads to a slowing down or vanished QBO, which could be avoided by some other injection strategies such as varying the injection area seasonally. However it is not straightforward to give any suggestion for alternative baseline

855 scenario for following studies or e.g next possible GeoMIP experiments, as SAI can be used to meet various different climate targets and none of the injection strategies can be optimized to meet all of the targets. In addition, there were e.g some changes in the mutual ranking in global mean forcing between studied scenarios, depending on injection rate. This is true especially when considering injection rates which can be considered "more realistic" (<10 $Tg(S)yr^{-1}$). In scenarios like G6sulfur, where injection rate varies, the most logical scenario for lower injection rates may not be the same as for higher injection rates. As

860 this study shows, the radiative forcing of certain injection strategies is also significantly dependent on the aerosol model. Thus there is a need for model intercomparison project using aerosol-climate models to simulate various SAI scenarios.

Here the simulations were done with a model configuration with fixed SST and the object was to analyze the impact of injection strategies and aerosol microphysical models on radiative forcing. The next step is to study how these radiative forcings translate to climate impacts, i.e changes in global and regional temperature and especially precipitation and if these responses

865 are dependent on the climate model. This will be studied in part 2.

Data availability. The data from the model simulations and implemented model codes are available from the authors upon request.

Appendix A: Simulations without nucleation

Our analyses in this study showed that model responses on stratospheric aerosol injection were significantly different between sectional aerosol model SALSA and modal aerosol scheme M7. Based on Fig. 4, this difference between the models is partly caused by how models solve the competition between new particle formation and condensation inside or near the injection regime. While injected sulfur tends to mainly form new particles in SALSA, in M7 sulfate condensates on pre-existing particles. To study the role of these differences on radiative forcing and particle size distribution we performed additional simulations where competition between nucleation and condensation were made consistent between the models. This was done by switching nucleation off, and emitting 25% of injected sulfur as $3\,\mathrm{nm}$ primary particles while the rest of the sulfur was injected as SO_2. Simulations were done for *Baseline* scenario with 2, 5, 20 and 50 Tg(S)yr^{-1} injections. By standardizing the competition between nucleation and condensation in SALSA and M7, the global mean SW radiative forcing, net radiative forcing and especially stratospheric sulfur burden between models are closer to each other than in the original setup (see Fig. A1). However, differences in the LW radiative forcings between models were slightly increased and the SW response was still significantly larger in SALSA than M7. Thus, the different treatment of the competition between nucleation and condensation explains the responses between models only partly. This is interesting especially because the zonal mean effective radius of stratospheric aerosols is consistent in these sensitivity simulation between models (See Fig. A2). However, a closer look on the aerosol size distribution inside the injection regime shows that even the effective radius were consistent between models, the size distribution is not. Generally, size distributions in simulations where nucleation is replaced by injecting 3nm primary aerosols are relatively similar to those in the original simulations, excluding the two smallest modes in M7 simulations (Fig. A3). The median size of nucleation (smallest) mode is larger, the number of Aitken mode (second smallest) aerosols is significantly higher and the median size is smaller than in the original simulations. Because of this, the effective radius of stratospheric aerosols is significantly smaller. However the aerosols in nucleation and Aitken mode do not have a notable impact on the radiation. As Fig. A3 shows, the two largest modes, accumulation and coarse, are relatively similar to those in the original simulations. There is still a large gap between these two modes, which is located at the size range of the largest backscattering efficiency. In addition, the number of coarse mode aerosols is even higher than with the original setup which explains the larger LW radiative forcing.

Overall, these simulations show that different radiative responses between the models are mainly originated from the representation of aerosols (sectional vs. modal), which were discussed in sect.3.2. In addition, this analysis shows that the effective radius is not always a representative measure for the size distribution and radiative impacts can be significantly different even in case of consistent effective radius.

Author contributions. AL designed the research, performed the experiments, carried out the analysis, and prepared the paper. All authors contributed ideas, participated in interpretation and discussion of the results, and contributed to writing the paper.
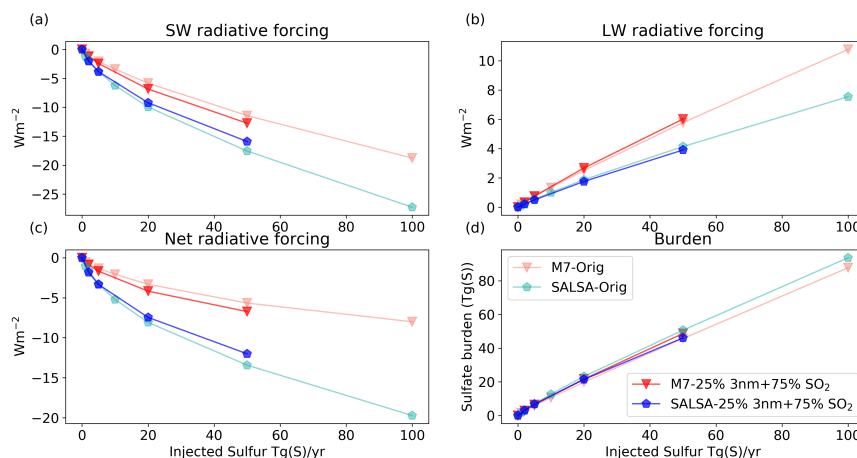
Figure A1. Global mean a) shortwave, b) longwave and c) total ~~radiative~~radiative forcing and d) stratospheric sulfate burden as a function of ~~injected sulfur~~injection rate. M7 results are shown by red lines and markers and SALSA results are indicated by blue color. Lighter dashed lines correspond original simulations and darker solid lines are representing corresponding simulations without the nucleation.
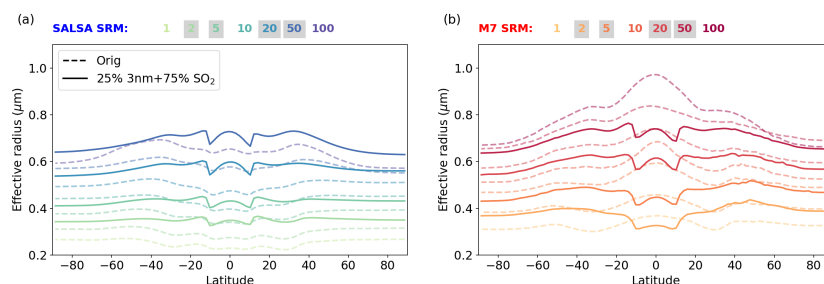
Figure A2. Zonal mean effective radius of stratospheric aerosols in different magnitude of sulfur injections simulated with a)SALSA and b) M7. Lighter dashed lines correspond original simulations and darker solid lines are representing corresponding simulations without the nucleation.

Competing interests. The authors declare that they have no conflict of interest.

Acknowledgements. The ECHAM-HAMMOZ model is developed by a consortium composed of ETHZ, Max-Planck Institut für Meteorologie, Forschungszentrum Jülich, the University of Oxford, and the Finnish Meteorological Institute; it is managed by the Center of Climate Systems Modeling (C2SM) at ETHZ.

Financial support. This research has been supported by the Tiina and Antti Herlin Foundation (grant no. 20190014 and 20200003). Ulrike Niemeier obtained support from the German DFG-funded Research Unit VollImpact FOR2820 grant no 398006378.

900
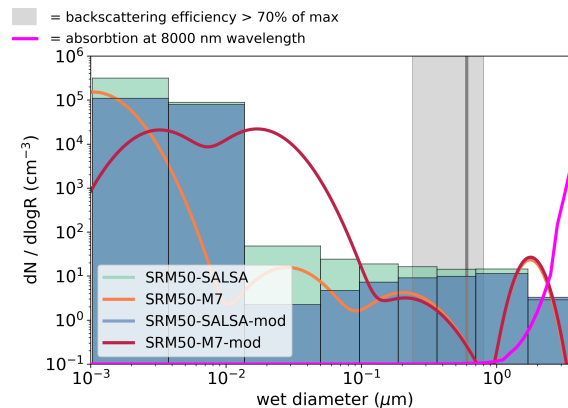
Figure A3. Aerosol number size distribution inside of injection regime in ~~scenarios SRM5 and~~ scenario SRM50 simulated with M7 and SALSA ~~without~~ in original simulations and simulations where the nucleation ~~. Dots on the top of the SALSA size bins are showing a mean diameter~~ is replaced by injecting 25% of ~~the bin~~ sulfur mass as 3nm primary particles. ~~Light green~~ The grey line shows to size of the maximum back scattering and shaded area indicates radius where aerosol backscattering is 70 % of maximum Dykema et al. (2016). Magenta line shows dependence of absorption of 8000nm wavelength on the (dry) size of the sulfate aerosols, based on the radiation module of SALSA.

References

Aswathy, V. N., Boucher, O., Quaas, M., Niemeier, U., Muri, H., Mülmenstädt, J., and Quaas, J.: Climate extremes in multi-model simulations of stratospheric aerosol and marine cloud brightening climate engineering, Atmospheric Chemistry and Physics, 15, 9593–9610, https://doi.org/10.5194/acp-15-9593-2015, https://acp.copernicus.org/articles/15/9593/2015/, 2015.

Bergman, T., Kerminen, V.-M., Korhonen, H., Lehtinen, K. J., Makkonen, R., Arola, A., Mielonen, T., Romakkaniemi, S., Kulmala, M., and Kokkola, H.: Evaluation of the sectional aerosol microphysics module SALSA implementation in ECHAM5-HAM aerosol-climate model, Geoscientific Model Development, 5, 845–868, https://doi.org/10.5194/gmd-5-845-2012, https://gmd.copernicus.org/articles/5/845/2012/, 2012.

Caldeira, K., Bala, G., and Cao, L.: The Science of Geoengineering, Annual Review of Earth and Planetary Sciences, 41, 231–256, https://doi.org/10.1146/annurev-earth-042711-105548, https://doi.org/10.1146/annurev-earth-042711-105548, 2013.

Chen, J.-P. and Lamb, D.: Simulation of Cloud Microphysical and Chemical Processes Using a Multicomponent Framework. Part I: Description of the Microphysical Model, Journal of Atmospheric Sciences, 51, 2613 – 2630, https://doi.org/10.1175/1520-0469(1994)051<2613:SOCMAC>2.0.CO;2, https://journals.ametsoc.org/view/journals/atsc/51/18/1520-0469_1994_051_2613_socmac_2_0_co_2.xml, 15 Sep. 1994.

Dykema, J. A., Keith, D. W., and Keutsch, F. N.: Improved aerosol radiative properties as a foundation for solar geoengineering risk assessment, Geophysical Research Letters, 43, 7758–7766, https://doi.org/10.1002/2016GL069258, https://agupubs.onlinelibrary.wiley.com/doi/abs/10.1002/2016GL069258, 2016.

English, J. M., Toon, O. B., and Mills, M. J.: Microphysical simulations of sulfur burdens from stratospheric sulfur geoengineering, Atmospheric Chemistry and Physics, 12, 4775–4793, https://doi.org/10.5194/acp-12-4775-2012, https://www.atmos-chem-phys.net/12/4775/2012/, 2012.

925 English, J. M., Toon, O. B., and Mills, M. J.: Microphysical simulations of large volcanic eruptions: Pinatubo and Toba, Journal of Geophysical Research: Atmospheres, 118, 1880–1895, https://doi.org/https://doi.org/10.1002/jgrd.50196, https://agupubs.onlinelibrary.wiley.com/doi/abs/10.1002/jgrd.50196, 2013.

Franke, H., Niemeier, U., and Visioni, D.: Differences in the quasi-biennial oscillation response to stratospheric aerosol modification depending on injection strategy and species, Atmospheric Chemistry and Physics, 21, 8615–8635, https://doi.org/10.5194/acp-21-8615-2021,
930   https://acp.copernicus.org/articles/21/8615/2021/, 2021.

Heckendorn, P., Weisenstein, D., Fueglistaler, S., Luo, B. P., Rozanov, E., Schraner, M., Thomason, L. W., and Peter, T.: The impact of geoengineering aerosols on stratospheric temperature and ozone, Environmental Research Letters, 4, 045 108, https://doi.org/10.1088/1748-9326/4/4/045108, https://doi.org/10.1088%2F1748-9326%2F4%2F4%2F045108, 2009.

Jacobson, M. Z.: Analysis of aerosol interactions with numerical techniques for solving coagulation, nucleation, condensation, dissolution,
935   and reversible chemistry among multiple size distributions, Journal of Geophysical Research: Atmospheres, 107, AAC 2–1–AAC 2–23, https://doi.org/10.1029/2001JD002044, https://agupubs.onlinelibrary.wiley.com/doi/abs/10.1029/2001JD002044, 2002.

Jones, A. C., Haywood, J. M., and Jones, A.: Climatic impacts of stratospheric geoengineering
with sulfate, black carbon and titania injection, Atmospheric Chemistry and Physics, 16, 2843–2862, https://doi.org/10.5194/acp-16-2843-2016, https://acp.copernicus.org/articles/16/2843/2016/, 2016.

940 Kerminen, V.-M. and Kulmala, M.: Analytical formulae connecting the "real" and the "apparent" nucleation rate and the nuclei number concentration for atmospheric nucleation events, Journal of Aerosol Science, 33, 609–622, https://doi.org/https://doi.org/10.1016/S0021-8502(01)00194-X, https://www.sciencedirect.com/science/article/pii/S002185020100194X, 2002.

Kleinschmitt, C., Boucher, O., and Platt, U.: Sensitivity of the radiative forcing by stratospheric sulfur geoengineering to the amount and strategy of the SO_2 injection studied with the LMDZ-S3A model, Atmospheric Chemistry and Physics, 18, 2769–2786,
945   https://doi.org/10.5194/acp-18-2769-2018, https://www.atmos-chem-phys.net/18/2769/2018/, 2018.

Kokkola, H., Hommel, R., Kazil, J., Niemeier, U., Partanen, A.-I., Feichter, J., and Timmreck, C.: Aerosol microphysics modules in the framework of the ECHAM5 climate model – intercomparison under stratospheric conditions, Geoscientific Model Development, 2, 97–112, https://doi.org/10.5194/gmd-2-97-2009, https://gmd.copernicus.org/articles/2/97/2009/, 2009.

Kokkola, H., Kühn, T., Laakso, A., Bergman, T., Lehtinen, K. E. J., Mielonen, T., Arola, A., Stadtler, S., Korhonen, H., Ferrachat, S.,
950   Lohmann, U., Neubauer, D., Tegen, I., Siegenthaler-Le Drian, C., Schultz, M. G., Bey, I., Stier, P., Daskalakis, N., Heald, C. L., and Romakkaniemi, S.: SALSA2.0: The sectional aerosol module of the aerosol–chemistry–climate model ECHAM6.3.0-HAM2.3-MOZ1.0, Geoscientific Model Development, 11, 3833–3863, https://doi.org/10.5194/gmd-11-3833-2018, https://www.geosci-model-dev.net/11/3833/2018/, 2018.

Kravitz, B., Robock, A., Tilmes, S., Boucher, O., English, J. M., Irvine, P. J., Jones, A., Lawrence, M. G., MacCracken, M., Muri, H.,
955   Moore, J. C., Niemeier, U., Phipps, S. J., Sillmann, J., Storelvmo, T., Wang, H., and Watanabe, S.: The Geoengineering Model Intercomparison Project Phase 6 (GeoMIP6): simulation design and preliminary results, Geoscientific Model Development, 8, 3379–3392, https://doi.org/10.5194/gmd-8-3379-2015, https://gmd.copernicus.org/articles/8/3379/2015/, 2015.

Kravitz, B., MacMartin, D. G., Wang, H., and Rasch, P. J.: Geoengineering as a design problem, Earth System Dynamics, 7, 469–497, https://doi.org/10.5194/esd-7-469-2016, https://esd.copernicus.org/articles/7/469/2016/, 2016.

960 Kravitz, B., MacMartin, D. G., Mills, M. J., Richter, J. H., Tilmes, S., Lamarque, J.-F., Tribbia, J. J., and Vitt, F.: First Simulations of Designing Stratospheric Sulfate Aerosol Geoengineering to Meet Multiple Simultaneous Climate Objectives, Journal of Geophysical

Research: Atmospheres, 122, 12,616–12,634, https://doi.org/10.1002/2017JD026874, https://agupubs.onlinelibrary.wiley.com/doi/abs/10.1002/2017JD026874, 2017.

Kravitz, B., MacMartin, D. G., Tilmes, S., Richter, J. H., Mills, M. J., Cheng, W., Dagon, K., Glanville, A. S., Lamarque, J.-F., Simpson, I. R., Tribbia, J., and Vitt, F.: Comparing Surface and Stratospheric Impacts of Geoengineering With Different SO2 Injection Strategies, Journal of Geophysical Research: Atmospheres, 124, 7900–7918, https://doi.org/https://doi.org/10.1029/2019JD030329, https://agupubs.onlinelibrary.wiley.com/doi/abs/10.1029/2019JD030329, 2019.

Kravitz, B., MacMartin, D. G., Visioni, D., Boucher, O., Cole, J. N. S., Haywood, J., Jones, A., Lurton, T., Nabat, P., Niemeier, U., Robock, A., Séférian, R., and Tilmes, S.: Comparing different generations of idealized solar geoengineering simulations in the Geoengineering Model Intercomparison Project (GeoMIP), Atmospheric Chemistry and Physics, 21, 4231–4247, https://doi.org/10.5194/acp-21-4231-2021, https://acp.copernicus.org/articles/21/4231/2021/, 2021.

Laakso, A., Kokkola, H., Partanen, A.-I., Niemeier, U., Timmreck, C., Lehtinen, K. E. J., Hakkarainen, H., and Korhonen, H.: Radiative and climate impacts of a large volcanic eruption during stratospheric sulfur geoengineering, Atmospheric Chemistry and Physics, 16, 305–323, https://doi.org/10.5194/acp-16-305-2016, https://acp.copernicus.org/articles/16/305/2016/, 2016.

Laakso, A., Korhonen, H., Romakkaniemi, S., and Kokkola, H.: Radiative and climate effects of stratospheric sulfur geoengineering using seasonally varying injection areas, Atmospheric Chemistry and Physics, 17, 6957–6974, https://doi.org/10.5194/acp-17-6957-2017, https://www.atmos-chem-phys.net/17/6957/2017/, 2017.

Laakso, A., Snyder, P. K., Liess, S., Partanen, A.-I., and Millet, D. B.: Differing precipitation response between solar radiation management and carbon dioxide removal due to fast and slow components, Earth System Dynamics, 11, 415–434, https://doi.org/10.5194/esd-11-415-2020, https://www.earth-syst-dynam.net/11/415/2020/, 2020.

McCusker, K. E., Battisti, D. S., and Bitz, C. M.: The Climate Response to Stratospheric Sulfate Injections and Implications for Addressing Climate Emergencies, Journal of Climate, 25, 3096 – 3116, https://doi.org/10.1175/JCLI-D-11-00183.1, https://journals.ametsoc.org/view/journals/clim/25/9/jcli-d-11-00183.1.xml, 01 May. 2012.

Mills, M. J., Richter, J. H., Tilmes, S., Kravitz, B., MacMartin, D. G., Glanville, A. A., Tribbia, J. J., Lamarque, J.-F., Vitt, F., Schmidt, A., Gettelman, A., Hannay, C., Bacmeister, J. T., and Kinnison, D. E.: Radiative and Chemical Response to Interactive Stratospheric Sulfate Aerosols in Fully Coupled CESM1(WACCM), Journal of Geophysical Research: Atmospheres, 122, 13,061–13,078, https://doi.org/https://doi.org/10.1002/2017JD027006, https://agupubs.onlinelibrary.wiley.com/doi/abs/10.1002/2017JD027006, 2017.

Naujokat, B.: An Update of the Observed Quasi-Biennial Oscillation of the Stratospheric Winds over the Tropics, Journal of Atmospheric Sciences, 43, 1873 – 1877, https://doi.org/10.1175/1520-0469(1986)043<1873:AUOTOQ>2.0.CO;2, https://journals.ametsoc.org/view/journals/atsc/43/17/1520-0469_1986_043_1873_auotoq_2_0_co_2.xml, 1986.

Niemeier, U. and Schmidt, H.: Changing transport processes in the stratosphere by radiative heating of sulfate aerosols, Atmospheric Chemistry and Physics, 17, 14 871–14 886, https://doi.org/10.5194/acp-17-14871-2017, https://acp.copernicus.org/articles/17/14871/2017/, 2017.

Niemeier, U. and Timmreck, C.: What is the limit of climate engineering by stratospheric injection of SO_2?, Atmospheric Chemistry and Physics, 15, 9129–9141, https://doi.org/10.5194/acp-15-9129-2015, https://www.atmos-chem-phys.net/15/9129/2015/, 2015.

Niemeier, U., Timmreck, C., Graf, H.-F., Kinne, S., Rast, S., and Self, S.: Initial fate of fine ash and sulfur from large volcanic eruptions, Atmospheric Chemistry and Physics, 9, 9043–9057, https://doi.org/10.5194/acp-9-9043-2009, https://acp.copernicus.org/articles/9/9043/2009/, 2009.

Niemeier, U., Schmidt, H., and Timmreck, C.: The dependency of geoengineered sulfate aerosol on the emission strategy, Atmospheric Science Letters, 12, 189–194, https://doi.org/10.1002/asl.304, https://rmets.onlinelibrary.wiley.com/doi/abs/10.1002/asl.304, 2011.

Niemeier, U., Richter, J. H., and Tilmes, S.: Differing responses of the quasi-biennial oscillation to artificial SO_2 injections in two global models, Atmospheric Chemistry and Physics, 20, 8975–8987, https://doi.org/10.5194/acp-20-8975-2020, https://acp.copernicus.org/articles/20/8975/2020/, 2020.

Niemeier, U., Riede, F., and Timmreck, C.: Simulation of ash clouds after a Laacher See-type eruption, Climate of the Past, 17, 633–652, https://doi.org/10.5194/cp-17-633-2021, https://cp.copernicus.org/articles/17/633/2021/, 2021.

Pierce, J. R., Weisenstein, D. K., Heckendorn, P., Peter, T., and Keith, D. W.: Efficient formation of stratospheric aerosol for climate engineering by emission of condensible vapor from aircraft, Geophysical Research Letters, 37, https://doi.org/10.1029/2010GL043975, https://agupubs.onlinelibrary.wiley.com/doi/abs/10.1029/2010GL043975, 2010.

Plazzotta, M., Séférian, R., Douville, H., Kravitz, B., and Tjiputra, J.: Land Surface Cooling Induced by Sulfate Geoengineering Constrained by Major Volcanic Eruptions, Geophysical Research Letters, 45, 5663–5671, https://doi.org/https://doi.org/10.1029/2018GL077583, https://agupubs.onlinelibrary.wiley.com/doi/abs/10.1029/2018GL077583, 2018.

Richter, J. H., Tilmes, S., Mills, M. J., Tribbia, J. J., Kravitz, B., MacMartin, D. G., Vitt, F., and Lamarque, J.-F.: Stratospheric Dynamical Response and Ozone Feedbacks in the Presence of SO2 Injections, Journal of Geophysical Research: Atmospheres, 122, 12,557–12,573, https://doi.org/https://doi.org/10.1002/2017JD026912, https://agupubs.onlinelibrary.wiley.com/doi/abs/10.1002/2017JD026912, 2017.

Schultz, M. G., Stadtler, S., Schröder, S., Taraborrelli, D., Franco, B., Krefting, J., Henrot, A., Ferrachat, S., Lohmann, U., Neubauer, D., Siegenthaler-Le Drian, C., Wahl, S., Kokkola, H., Kühn, T., Rast, S., Schmidt, H., Stier, P., Kinnison, D., Tyndall, G. S., Orlando, J. J., and Wespes, C.: The chemistry–climate model ECHAM6.3-HAM2.3-MOZ1.0, Geoscientific Model Development, 11, 1695–1723, https://doi.org/10.5194/gmd-11-1695-2018, https://www.geosci-model-dev.net/11/1695/2018/, 2018.

Smith, W. and Wagner, G.: Stratospheric aerosol injection tactics and costs in the first 15 years of deployment, Environmental Research Letters, 13, 124 001, https://doi.org/10.1088/1748-9326/aae98d, https://doi.org/10.1088/1748-9326/aae98d, 2018.

Stevens, B., Giorgetta, M., Esch, M., Mauritsen, T., Crueger, T., Rast, S., Salzmann, M., Schmidt, H., Bader, J., Block, K., Brokopf, R., Fast, I., Kinne, S., Kornblueh, L., Lohmann, U., Pincus, R., Reichler, T., and Roeckner, E.: Atmospheric component of the MPI-M Earth System Model: ECHAM6, Journal of Advances in Modeling Earth Systems, 5, 146–172, https://doi.org/10.1002/jame.20015, https://agupubs.onlinelibrary.wiley.com/doi/abs/10.1002/jame.20015, 2013.

Sukhodolov, T., Sheng, J.-X., Feinberg, A., Luo, B.-P., Peter, T., Revell, L., Stenke, A., Weisenstein, D. K., and Rozanov, E.: Stratospheric aerosol evolution after Pinatubo simulated with a coupled size-resolved aerosol–chemistry–climate model, SOCOL-AERv1.0, Geoscientific Model Development, 11, 2633–2647, https://doi.org/10.5194/gmd-11-2633-2018, https://gmd.copernicus.org/articles/11/2633/2018/, 2018.

Tegen, I., Neubauer, D., Ferrachat, S., Siegenthaler-Le Drian, C., Bey, I., Schutgens, N., Stier, P., Watson-Parris, D., Stanelle, T., Schmidt, H., Rast, S., Kokkola, H., Schultz, M., Schroeder, S., Daskalakis, N., Barthel, S., Heinold, B., and Lohmann, U.: The global aerosol–climate model ECHAM6.3–HAM2.3 – Part 1: Aerosol evaluation, Geoscientific Model Development, 12, 1643–1677, https://doi.org/10.5194/gmd-12-1643-2019, https://www.geosci-model-dev.net/12/1643/2019/, 2019.

Tilmes, S., Fasullo, J., Lamarque, J.-F., Marsh, D. R., Mills, M., Alterskjær, K., Muri, H., Kristjánsson, J. E., Boucher, O., Schulz, M., Cole, J. N. S., Curry, C. L., Jones, A., Haywood, J., Irvine, P. J., Ji, D., Moore, J. C., Karam, D. B., Kravitz, B., Rasch, P. J., Singh, B., Yoon, J.-H., Niemeier, U., Schmidt, H., Robock, A., Yang, S., and Watanabe, S.: The hydrological impact of geoengineering in

the Geoengineering Model Intercomparison Project (GeoMIP), Journal of Geophysical Research: Atmospheres, 118, 11,036–11,058, https://doi.org/https://doi.org/10.1002/jgrd.50868, https://agupubs.onlinelibrary.wiley.com/doi/abs/10.1002/jgrd.50868, 2013.

Tilmes, S., Richter, J. H., Kravitz, B., MacMartin, D. G., Mills, M. J., Simpson, I. R., Glanville, A. S., Fasullo, J. T., Phillips, A. S., Lamarque, J.-F., Tribbia, J., Edwards, J., Mickelson, S., and Ghosh, S.: CESM1(WACCM) Stratospheric Aerosol Geoengineering Large Ensemble Project, Bulletin of the American Meteorological Society, 99, 2361 – 2371, https://doi.org/10.1175/BAMS-D-17-0267.1, https://journals.ametsoc.org/view/journals/bams/99/11/bams-d-17-0267.1.xml, 2018a.

Tilmes, S., Richter, J. H., Mills, M. J., Kravitz, B., MacMartin, D. G., Garcia, R. R., Kinnison, D. E., Lamarque, J.-F., Tribbia, J., and Vitt, F.: Effects of Different Stratospheric SO2 Injection Altitudes on Stratospheric Chemistry and Dynamics, Journal of Geophysical Research: Atmospheres, 123, 4654–4673, https://doi.org/10.1002/2017JD028146, https://agupubs.onlinelibrary.wiley.com/doi/abs/10.1002/2017JD028146, 2018b.

Toohey, M., Krüger, K., Niemeier, U., and Timmreck, C.: The influence of eruption season on the global aerosol evolution and radiative impact of tropical volcanic eruptions, Atmospheric Chemistry and Physics, 11, 12 351–12 367, https://doi.org/10.5194/acp-11-12351-2011, https://acp.copernicus.org/articles/11/12351/2011/, 2011.

Vattioni, S., Weisenstein, D., Keith, D., Feinberg, A., Peter, T., and Stenke, A.: Exploring accumulation-mode H_2SO_4 versus SO_2 stratospheric sulfate geoengineering in a sectional aerosol–chemistry–climate model, Atmospheric Chemistry and Physics, 19, 4877–4897, https://doi.org/10.5194/acp-19-4877-2019, https://www.atmos-chem-phys.net/19/4877/2019/, 2019.

Vignati, E., Wilson, J., and Stier, P.: M7: An efficient size-resolved aerosol microphysics module for large-scale aerosol transport models, Journal of Geophysical Research: Atmospheres, 109, https://doi.org/https://doi.org/10.1029/2003JD004485, https://agupubs.onlinelibrary.wiley.com/doi/abs/10.1029/2003JD004485, 2004.

Visioni, D., MacMartin, D. G., Kravitz, B., Tilmes, S., Mills, M. J., Richter, J. H., and Boudreau, M. P.: Seasonal Injection Strategies for Stratospheric Aerosol Geoengineering, Geophysical Research Letters, 46, 7790–7799, https://doi.org/https://doi.org/10.1029/2019GL083680, https://agupubs.onlinelibrary.wiley.com/doi/abs/10.1029/2019GL083680, 2019.

Visioni, D., MacMartin, D. G., Kravitz, B., Lee, W., Simpson, I. R., and Richter, J. H.: Reduced Poleward Transport Due to Stratospheric Heating Under Stratospheric Aerosols Geoengineering, Geophysical Research Letters, 47, e2020GL089 470, https://doi.org/https://doi.org/10.1029/2020GL089470, https://agupubs.onlinelibrary.wiley.com/doi/abs/10.1029/2020GL089470, e2020GL089470 10.1029/2020GL089470, 2020a.

Visioni, D., Slessarev, E., MacMartin, D. G., Mahowald, N. M., Goodale, C. L., and Xia, L.: What goes up must come down: impacts of deposition in a sulfate geoengineering scenario, Environmental Research Letters, 15, 094 063, https://doi.org/10.1088/1748-9326/ab94eb, https://doi.org/10.1088%2F1748-9326%2Fab94eb, 2020b.

Visioni, D., MacMartin, D. G., and Kravitz, B.: Is Turning Down the Sun a Good Proxy for Stratospheric Sulfate Geoengineering?, Journal of Geophysical Research: Atmospheres, 126, e2020JD033 952, https://doi.org/https://doi.org/10.1029/2020JD033952, https://agupubs.onlinelibrary.wiley.com/doi/abs/10.1029/2020JD033952, e2020JD033952 2020JD033952, 2021.

Wan, H., Rasch, P. J., Zhang, K., Kazil, J., and Leung, L. R.: Numerical issues associated with compensating and competing processes in climate models: an example from ECHAM-HAM, Geoscientific Model Development, 6, 861–874, https://doi.org/10.5194/gmd-6-861-2013, https://gmd.copernicus.org/articles/6/861/2013/, 2013.

Young, K. C.: A Numerical Simulation of Wintertime, Orographic Precipitation: Part I. Description of Model Microphysics and Numerical Techniques, Journal of Atmospheric Sciences, 31, 1735 – 1748, https://doi.org/10.1175/1520-0469(1974)031<1735:ANSOWO>2.0.CO;2, https://journals.ametsoc.org/view/journals/atsc/31/7/1520-0469_1974_031_1735_answo_2_0_co_2.xml, 01 Oct. 1974.

Yu, X., Moore, J. C., Cui, X., Rinke, A., Ji, D., Kravitz, B., and Yoon, J.-H.: Impacts, effectiveness and regional inequalities of the GeoMIP G1 to G4 solar radiation management scenarios, Global and Planetary Change, 129, 10–22, https://doi.org/https://doi.org/10.1016/j.gloplacha.2015.02.010, https://www.sciencedirect.com/science/article/pii/S0921818115000569, 2015.

Zhang, K., O'Donnell, D., Kazil, J., Stier, P., Kinne, S., Lohmann, U., Ferrachat, S., Croft, B., Quaas, J., Wan, H., Rast, S., and Feichter, J.: The global aerosol-climate model ECHAM-HAM, version 2: sensitivity to improvements in process representations, Atmospheric Chemistry and Physics, 12, 8911–8949, https://doi.org/10.5194/acp-12-8911-2012, https://www.atmos-chem-phys.net/12/8911/2012/, 2012.